chips

MDPI

Review

An Overview of State-of-the-Art D-Band Radar System Components

Pascal Stadler [1,*], Hakan Papurcu [1], Tobias Welling [1], Simón Tejero Alfageme [2] and Nils Pohl [1,3]

[1] Institute of Integrated Systems, Ruhr-University Bochum, Universitätsstr. 150, D-44801 Bochum, Germany
[2] Huawei Technologies Duesseldorf GmbH, Riesstrasse 25, D-80922 Munich, Germany
[3] Fraunhofer FHR, Fraunhoferstr. 20, D-53343 Wachtberg, Germany
* Correspondence: pascal.stadler@ruhr-uni-bochum.de

Abstract: In this article, a literature study has been conducted including 398 radar circuit elements from 311 recent publications (mostly between 2010 and 2022) that have been reported mainly in the F-, D- and G-Band (80–200 GHz). This study is intended to give a state-of-the-art comparison on the performance of the different technologies—RFCMOS, SiGe/BiCMOS and III–V semiconductor composites—regarding the most crucial circuit parameters of Voltage-Controlled Oscillators (VCO), Power Amplifiers (PA), Phase Shifters (PS), Low-Noise Amplifiers (LNA) and Mixers. The most common topologies of each circuit element as well as the differences between the technolgies will futher be laid out while reasoning their benefits. Since not all devices were derived solely from single device publications, necessary steps to yield as fairly a comparison as possible were taken. Results include the area and power efficiency in RFCMOS, superior noise and power performance in III–V semiconductors and a continuous compromise between efficiency and performance in SiGe. The most rarely published devices, being Mixers and PSs, in the given frequency range have also been identified to give incentive for further developments.

Keywords: III–V semiconductor; D-Band; F-Band; G-Band; Low-Noise Amplifier; Mixer; Phase Shifter; Power Amplifier; radar circuits; RFCMOS; SiGe

Citation: Stadler, P.; Papurcu, H.; Welling, T.; Alfageme, S.; Pohl, N. An Overview of State-of-the-Art D-Band Radar System Components. *Chips* **2022**, *1*, 121–149. https://doi.org/10.3390/chips1030009

Academic Editor: Gaetano Palumbo

Received: 24 August 2022
Accepted: 19 September 2022
Published: 21 September 2022

1. Introduction

A lot of scientific interest has been invested in the D-Band in the last few years due to its relatively low atmospheric attenuation [1] at high frequencies. This is exploited by novel D-Band systems in the unregulated ISM-Band (122–123 GHz) [2], the potential automotive-band (134–141 GHz) [3] and various, recently FCC, Ofcom as well as CEPT/ETSI-approved industrial frequency bands above 100 GHz [4]. Especially radar systems have grown in significance, as they have been used in different applications such as imaging, near-field communications, wireless personal area networks or distance/velocity measurements [5–8]. This increased demand facilitated not only continuous scaling of technologies such as RFCMOS, SiGe HBT or III–V semiconductor composites (e.g., InP or GaAs) but also led to higher transit (ct. Figure 1) and oscillation frequencies.

Furthermore, these technologies are supported by new advances in packaging such as Wafer-Level Packaging (WLP) [9], allowing for more reliability whilst increasing the performance not only for single- but also multi-technology systems compared to wire-bond techniques.

To oversee new progress in the multitude of different devices published each year, surveys such as [10,11] have been conducted. They, however, only focus on single device publications for a specific circuit element, leaving out its performance in radar systems. As a result, this overview is meant to present the current state-of-the-art performance of all devices that are crucial for a radar system in the mentioned technologies around 140 GHz.

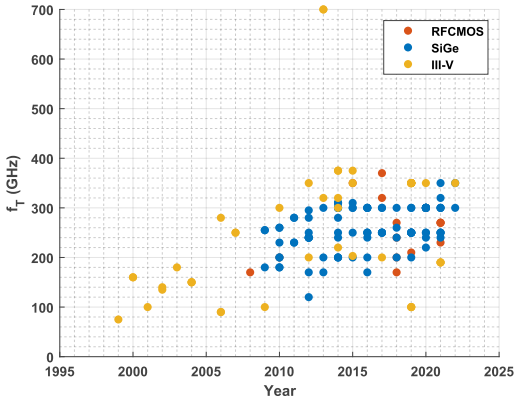

Figure 1. Development of f_T from the investigated publications over time. The frequency range of the devices totals: 13.895–208.55 GHz.

2. Radar Circuit Elements

Universally, radar systems are composed of a signal source and at least one transmit (Tx) and one receive path (Rx). A Voltage-Controlled Oscillator (VCO) generally locked in a Phase-Locked Loop (PLL) constitutes the signal source. The frequency-stabilized signal has either a static frequency as is the case for Continuous Wave (CW) or will be modulated for Frequency-Modulated Continuous Wave (FMCW) applications. Depending on the frequency of the VCO and the amount of Tx/Rx channels, frequency multiplication and distribution networks are required. Both have been omitted from this study, because their shortcomings can be compensated by buffer stages and the data can be adjusted theoretically.

A Tx primarily focuses on delivering as much power as possible to antennas in order to increase the Link Budget (LB) of the sytem as stated by the radar equation [12]:

$$\mathrm{LB} = \frac{\mathrm{P_{Rx}}(r)}{\mathrm{S_i}},$$

$$\mathrm{P_{Rx}}(r) = \frac{\mathrm{P_{Tx}G_{Tx}G_{Rx}}\lambda^2\sigma_{\mathrm{Antenna}}}{(4\pi)^3\mathrm{r}^4}. \tag{1}$$

For this reason, a Power Amplifier (PA), divided into different stages, and/or multiple PAs combined in parallel (power combining) are used. The succeeding antennas might have to be driven with different phases in Multiple Input Multiple Output (MIMO) radars to enlarge the virtual array size or achieve beamsteering capabilities. This can be completed by applying phase shifters (PSs).

Owing to a typically low signal level caused by the free space loss (Equation (1)), the received signal ought to be amplified. A Low-Noise Amplifier (LNA) is usually employed for this purpose to retain a high Signal to Noise Ratio, which is the result of the LNA's low noise contribution and the reduced noise impact of all following elements. Lastly, the frequency of the amplified signal is downconverted to a lower-frequency range for digital signal processing typically by utilizing the VCO signal at a Mixers Local Oscillator input.

All previously mentioned circuit elements will be separately investigated in the following sections.

2.1. Voltage-Controlled Oscillator (VCO)

A VCO is a circuit element that changes its output frequency depending on the applied tuning voltage. Unlike the other circuit elements in this overview, it is not necessarily employed at D-Band frequencies but rather at lower frequencies to decrease the VCOs complexity and ensure correct operation with improved performance. The subsequent lower frequency signal is then upconverted by frequency multipliers such as doubler or

tripler architectures. A radar operating frequencies therefore depends on the frequency multiplied carrier frequency f_c and the Frequency Tuning Range (FTR) [12]:

$$\mathrm{FTR} = \frac{f_{max} - f_{min}}{f_c} \cdot 100\% \tag{2}$$

of the VCO. As FTR stays constant regardless of the operating frequency, it can be used to compare the tunability of VCOs in the D-Band. Figure 2 displays the FTR for all gathered VCOs where each unique shape represents a different topology according to given legend. Exemplary VCOs were collected outside the F-, D- or G-Band to give an estimation of VCOs at lower frequencies. A decreasing trend of FTR with f_c can be determined. Additionally, the technologies are primarily distributed in specific frequency bands such as the K-/E-Band for RFCMOS, the U-/W-Band for III–V semiconductors or the Ka-/D-Band for SiGe. Based on the lack of SiGe in the W-Band, this is likely a statistical artifact emerging from publications not being sought out excessively below the F-Band.

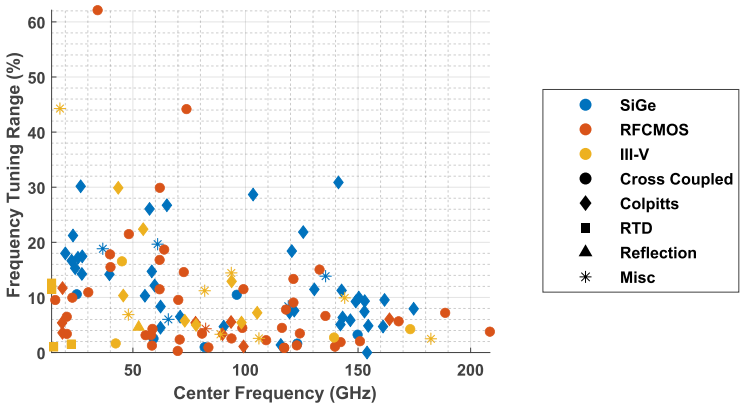

Figure 2. VCO: Frequency Tuning Range as function of the Center Frequency in the frequency range of 13.895–208.55 GHz.

The most dominant characteristic to assess a VCO on is the Phase Noise (PN). It describes the intensity of undesired frequency components in relation to f_c and is therefore measured in dbc/Hz [12]. These undesired frequency components might be downconverted or emitted, worsening the detectability of radar targets. Due to the exponential drop in PN starting from the f_c, it is imperative to use equal Offset Frequencies and Measurement Bandwidths when comparing VCOs. Offset Frequencies of 1 MHz and Measurement Bandwidths of 1 Hz were collected whenever possible. When the PN of all collected VCOs in Figure 3 is inspected, a distinct frequency dependency is visible. The higher the frequency, the more PN is generally introduced into the system. As a result, one might assume that frequency multiplied low frequency oscillations perform better than higher frequency signals. That assumption, however, does not take the added phase noise due to frequency multiplication into account. If a Frequency Multiplication Factor N were to be defined as:

$$\mathrm{N} = \frac{f_{target}}{f_c}, \tag{3}$$

the according PN addition to reach the desired frequency f_{target} can be derived to be [13]:

$$\Delta\mathrm{L}(\mathrm{N}\omega_0) = \Delta\mathrm{L}(\omega_0) + 20 \cdot Log_{10}(\mathrm{N}). \tag{4}$$

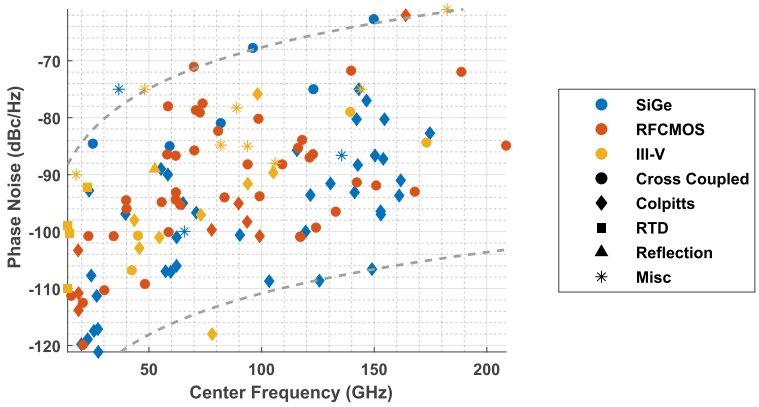

Figure 3. VCO: Phase Noise as a function of the Center Frequency. Dashed lines mark the $\pm 2\sigma$ interval in accorance with Leeson's equation.

To put it into perspective, 6 dBc/Hz of PN is added per doubler and 9.5 dBc/Hz is added per tripler stage. It should be pointed out here that SiGe and RFCMOS publications readily make use of push–push doublers to achieve higher operating frequencies while attenuating the fundamental $f_c/2$ as well as odd harmonics $(2n+1) \cdot f_c/2, \forall n = \mathbb{N}$. Since the doublers' non-ideal contribution cannot be removed, nor the losses estimated, they will not be accounted for rather but seen as a part of a higher frequency VCO. A more comprehensible illustration of the corrected PN alongside the mean PN of the specific technologies is given in Figure 4 for a f_{target} of 140 GHz. From it, an increase in Phase Noise of about 3 dB is present on average between SiGe (−89.46 dBc/Hz), RFCMOS (−86.56 dBc/Hz) and III–V semiconductor composites (−83.32 dBc/Hz). By examining the value spread, one can determine the consistency of the PN performance. SiGe has a larger span, whereas RFCMOS and III–V semiconductors display more reliable values.

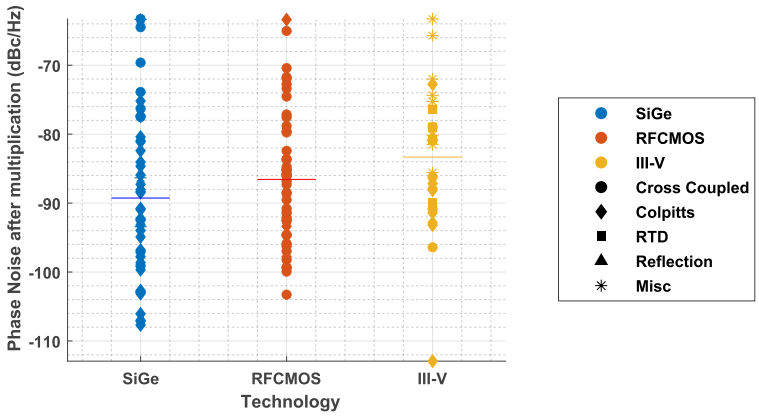

Figure 4. VCO: Phase Noise adjusted by the required multiplication stages to reach 140 GHz. Horizontal lines represent mean values.

Another important trait of VCOs is the Output Power P_{Out} that is shown alongside the DC-Power Consumption P_{DC} in Figure 5. High P_{Out} allows for less/no buffer stages to be used to compensate potential losses. These buffer stages would also generate noise, which can be largely disregarded as it is Amplitude Noise and not Phase Noise [14]. It has to be noted that the presence of buffer stages, that could not be de-embedded, might result in the data instead reflecting on the performance of those buffers. Nonetheless, a linear relation between P_{Out} and P_{DC} is apparent. Higher P_{Out} thus necessitates a higher P_{DC}. Moreover, the technologies evidently differ in DC-Power. The lower spectrum of Figure 5 is almost entirely made up of RFCMOS devices, whereas higher P_{DC} are seen first in SiGe and then in III–V semiconductors.

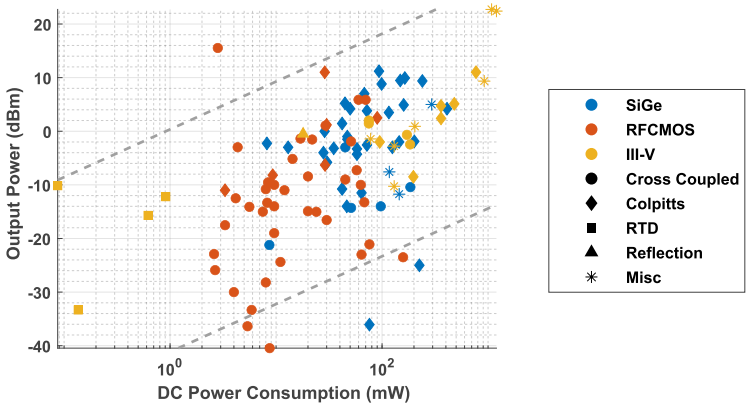

Figure 5. VCO: Output Power as a function of the DC-Power Consumption in the frequency range of 13.895–208.55 GHz. Dashed lines mark the $\pm 2\sigma$ interval.

A consideration of the topology leads to a vastly dissimilar circuit structure between VCOs from different technologies. Whereas RFCMOS heavily favors a cross-coupled structure as a result of an easy start-up with lower power consumption (cf. Figure 5), SiGe uses its higher transconductance gm to drive colpitts/hartley VCOs that usually have better noise and power performance (Figures 3–5) [15,16]. Considering that a decent number of III–V semiconductor VCOs could only be gathered prior to 2010 (see Figure 1), a lot of miscellaneous (Misc) circuit concepts were found alongside the prevalent cross-coupled and colpitts structure. Of additional note in this case are Resonate Tunneling Diode (RTD)-based VCOs that allow for extremely low-power oscillations (ct. Figure 5) when a low voltage is applied [17]. Another interesting detail is exposed when the varactor of the technologies is inspected. While the respective transistor type is used in RFCMOS (MOS-varactor) and III–V semiconductors (HBT/HEMT-varactor), SiGe HBT VCOs are commonly seen using MOS-varactors. This is mainly due to MOS-varactors having a comparable Q-factor as well as no imminent danger to forward bias pn-junctions at low Tuning Voltages [18].

2.2. Power Amplifier (PA)

PAs are typically driven in saturation, if no amplitude modulation is required, to generate a constant high Output Power P_{sat}. P_{sat} is generated by an average of 3.07/3.46/3.65 PA stages in SiGe/RFCMOS/III–V semiconductors, which are divided into multiple buffer/gain stages and an output stage. Generally, both stage types are of a similar kind of topology, which is why buffer/gain stages will not be touched on further.

A commonly used circuit modification to increase the Output Power is to connect multiple PAs in parallel (power combining). Power combining takes the form of either transmission line- or transformer-based combining, depending on the technology that is used. Resulting from the relatively low Q-factor of passive structures in RFCMOS, transformers are not only used to connect the different PA stages but also to link parallel PAs. This has the added benefit of a spacially low power increase. Two different transformer combining variants can be distinguished, being voltage- and current combining. Voltage combining uses one coil to enclose both load coils of the parallel PAs, whereas current combining employs a coil for each load coil with one terminal shorted to ground. The low output impedance provided by voltage combining is favored at lower frequencies in contrast to the lower parasitic influence of current combining at higher frequencies [19]. Moreover, different turn ratios allow for offsetting the restrictions of current combining, resulting in no voltage combiner being used in the whole dataset. For the other technologies, transmission-line based combining such as Wilkinson dividers/combiners were almost exclusively used. This has likely to do with the high area consumption of transformers.

In terms of the added Output Power, power combining does not reflect on the employed technology, instead adding $3\,\mathrm{dB} \cdot Log_2(\mathrm{N})$ assuming N lossless, parallel and saturated stages. Its ideal contribution has consequently been removed in Figure 6, which also

displays the mean P_{sat} of each technology ($\overline{P_{sat,SiGe}} = 11.82\,dBm$, $\overline{P_{sat,RFCMOS}} = 8.67\,dBm$, $\overline{P_{sat,III-V}} = 15.16\,dBm$). III–V semiconductor components deliver a higher output power than its two competitors. Its data points are also moderately grouped up, ensuring usually high P_{sat} in these devices. Likely by virtue of parity issues in III–V semiconductors, single-ended structures make up the majority its publications. Benefits of differential techniques such as the increased Common-Mode-Rejection Ratio (CMRR) are therefore not present in III–V semiconductor PAs. A low variation and thus reliable values are also seen in RFCMOS alongside modest P_{sat}. This comparatively low P_{sat} can largely be attributed to low breakdown voltages, which necessitate lower gain and deep-well processes for cascode structures [20–23]. Thus, the Miller effect is canceled, and the stability is increased through neutralization capacitance in common source/emitter (CS) circuits instead [24]. In contrast, mainly cascode stages to suppress the Miller effect and leverage the high gm of SiGe let it compete with both technologies as a result of larger deviations from its mean [25–28].

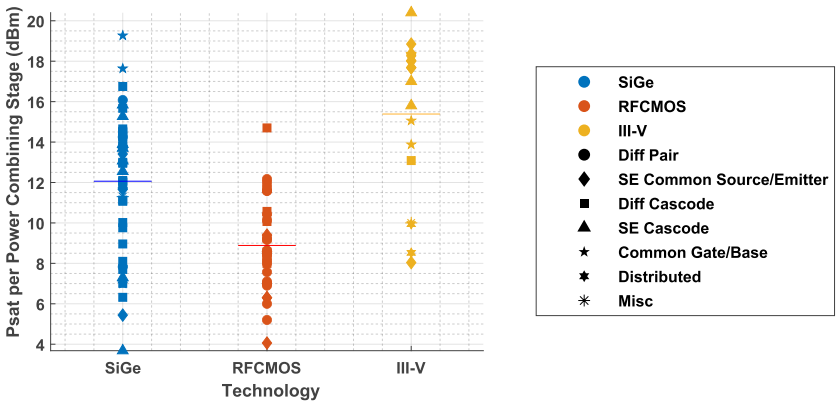

Figure 6. PA: Psat per power combining stage in the frequency range of 90–190 GHz. Horizontal lines represent mean values.

A high P_{sat} in a PA can only be considered a merit if it is accompanied by a sufficiently high enough amplification factor (Gain). It is mostly reported as the Small Signal Gain, i.e., the Gain in the linear region. Although not specifically noted here, the Gain-Bandwidth Product is also commonly used to express the Gain of a PA. Since the bandwidth could not be estimated with enough certainty, it was left out of this study. Nevertheless, distributed amplifiers can be highlighted as having the highest recorded bandwidths. When the Gain is set into relation with the DC Power Consumption (Figure 7), it is customarily compiled into a different criterion called the Power-Added Efficiency PAE [29]:

$$PAE = \frac{P_{in} \cdot (Gain - 1)}{P_{DC}} \cdot 100\,\% = \frac{P_{out} - P_{in}}{P_{DC}} \cdot 100\,\% \tag{5}$$

to estimate the efficiency of PAs. From Figure 8, RFCMOS devices can be deduced as having the highest PAE in their respective P_{sat} region. The next highest efficiency is displayed in SiGe. Yet, to achieve the highest P_{sat}, III–V semiconductor composites become indispensable. From a closer inspection of Figure 8, common base/gate (CB) stages emerge as one of the best topologies for high P_{sat}. The reason behind this, as is explained in [30], is that CB stages grow more efficient than common emitter stages as the Operating Frequency approaches f_T. f_T conversely is strongly dependant on the current density j_C and thus P_{sat} by prospect of the linear relation between P_{sat} and P_{DC}. The improved efficiency added to a non-class A operation facilitates low power consumption, thus yielding high PAE.

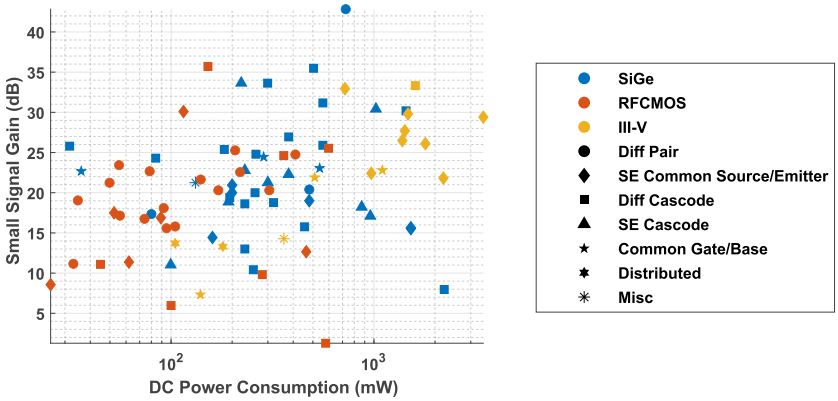

Figure 7. PA: Gain as a function of the DC Power Consumption in the frequency range of 90–190 GHz.

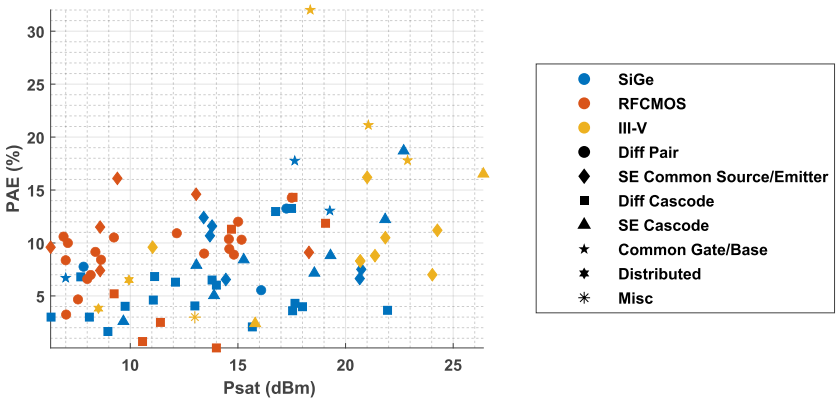

Figure 8. PA: PAE as a function of Psat in the frequency range of 90–190 GHz.

In cases where modulation (e.g., in communication systems) of the emitted signal is relevant, linearity becomes one of the focal points of PAs. A heavily used criterion is the First-Order Compression Point (P1dB), which can be further divided into an Output Referred (OP1dB) or an Input Referred Compression Point (IP1dB). It references a 1 dB variation between the course of the output power and the extrapolation of the linear region. Albeit the OP1dB is typically of higher interest for PAs, both compression points are given in Figure 9. An analysis of the technologies yields increased linearity in III–V semiconductors compared to SiGe and SiGe compared to RFCMOS. In terms of topology, the highest linearity is seen in single-ended devices.

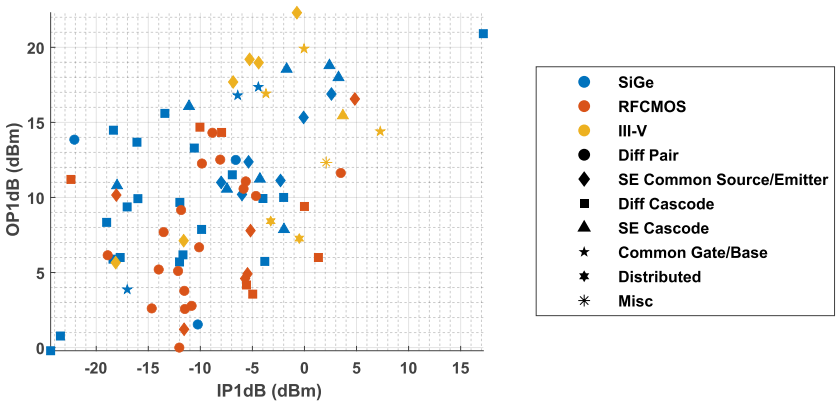

Figure 9. PA: Linearity shown in OP1dB vs. IP1dB from 90–190 GHz.

2.3. Phase Shifter (PS)

The phase of a signal can be adjusted by applying either a passive, reflective or vector modulated (VM) PS. The different architectures mainly differ in terms of Resolution, Gain and linearity. Active VM-PSs generally have a higher Resolution and Gain [31], whereas the linearity in the passive architectures is higher [32]. Since the Resolution is intrinsically linked to the utilized bitwidth of PSs, Figure 10 only shows the Gain of the reported PSs.

The bulk of the data, especially for RFCMOS, was accumulated in the lower F- and higher W-Band on the account that only a few PS were reported in the D-Band. The scarcity of the data allows for no conclusive performance statements. Only passive phase shifters, divided into Reflection-Type Phase Shifters (RTPS) and switched passive elements, were reported for III–V semiconductors, whereas a greater number of active devices are present for the other technologies. These active components can largely be divided into two subcategories: Switched-Quad (the sole VM-PS in RFCMOS) and Vector-Sum (exclusively present in SiGe). They differ from each other simply by their polarity/phase selection. While the digital select signals are directly applied at the Gate/Base of the switching Quads (akin to setting VDD to a Gilber–Cell transistor quad), vector summing involves numerous selections by SPDT-Switches and phase shifts by a multitude of couplers. Additionally, multiple Vector-Gain Amplifiers (VGA) to sufficiently cover the coupler losses as well as provide adequate resolutions are required. The Resolution and Gain of switching quads depend on the number of quads or pre-amplifiers used, which will not be covered in this study. As for the differences between RFCMOS and SiGe, a similar average Gain in the examined frequency bands is exhibited. For the same frequency range, however, SiGe outperforms RFCMOS.

In order to assess the phase and amplitude imbalances in each PS state, Root Mean Square (RMS) errors are most commonly used. Both the RMS Gain as well as the RMS Phase Errors are depicted in Figure 11. Disproportionally higher Phase Errors in RFCMOS and Gain errors in SiGe were reported when comparing the technologies. These devices almost exclusively belong to the vector-sum/switched-quad PSs for SiGe/RFCMOS. Thus, it can be estimated that the complexity in those devices is at fault for their poor RMS errors. The other devices and especially the passive devices in III–V composite devices, with its only poor performing device being an outlier, accomplished low RMS errors.

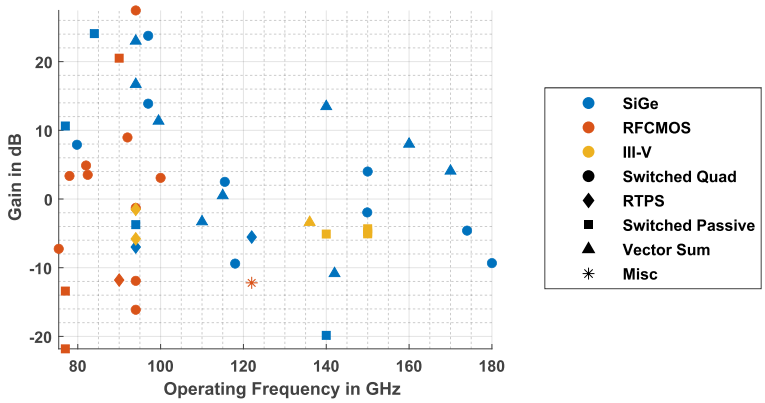

Figure 10. PS: Gain as a function of the frequency.

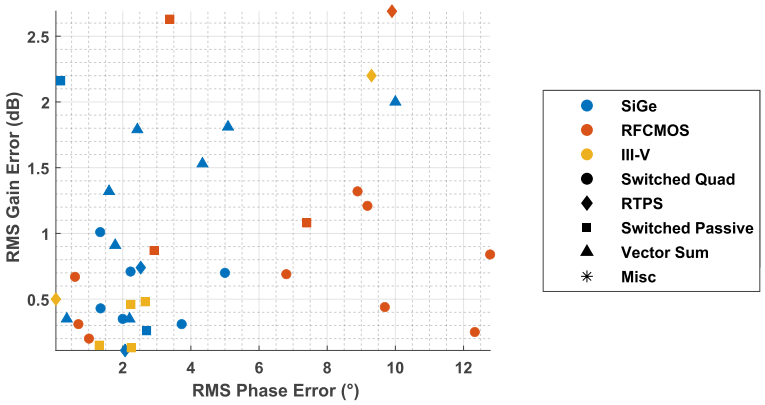

Figure 11. PS: RMS Gain and Phase Error in the frequency range of 75.4–180 GHz.

2.4. Low-Noise Amplifier (LNA)

As the first active element in the receiver chain, the LNA's noise contribution F_1 has the strongest impact on a system's Noise Figure (NF) in accordance with Friis' formula [12]:

$$NF_{receiver} = 10 \cdot Log_{10}\left(F_1 + \sum_{i=2}^{n} \frac{F_i - 1}{\prod_{j=1}^{i-1} Gain_j}\right). \quad (6)$$

This noise contribution differs noticeably between III–V semiconductors and both SiGe and RFCMOS as is evident from Figure 12. On average, the lowest Noise Figure can be achieved in III–V semiconductors ($\overline{NF_{III-V}} = 3.67$ dB). In contrast to the other two technologies, only single-ended amplifiers were used because they exhibit better noise performance than differential ones. RFCMOS and SiGe devices in comparison show an almost equal NF with the former having a higher discrepancy and thus yielding slightly worse average values ($\overline{NF_{RFCMOS}} = 7.77$ dB) compared to latter ($\overline{NF_{SiGe}} = 7.48$ dB). Another important NF contributor is the interconnects in each technology. While low loss/noise Grounded-Coplanar Wave Guides (GCPW) are commonly used in III–V semiconductors, transformer and transmission line losses in RFCMOS and SiGe, respectively, may increase their NF.

While F_1 does not become reduced by any other circuit element, an LNA decreases the noise contribution F_i of all following elements by its Conversion Gain (CG) as stated in Equation (6). Usually, a compromise between the LNAs NF and the Gain, as Figure 13 illustrated, has to be carried out. This compromise also appears in the choice of topology wherein the increased Gain of a cascode stage worsens the NF due to the contribution of the common base/gate stage when contrasted with common source/emitter (CS) stages [33–35]. To offset the Gain difference, more stages are usually employed in CS LNAs [36]. This leads to the least amount of Gain stages (1–4 stages) being used in SiGe devices with 2.74 stages on average, even though among the highest Gains were demonstrated. In stark contrast, RFCMOS has the largest span with 1–8 stages and a mean stage amount of 3.96, while the overall lowest CG was repeatedly reported. Lastly, III–V semiconductors can be highlighted as having the best mean Gain whilst averaging 3.71 stages within a range of 2–4 stages.

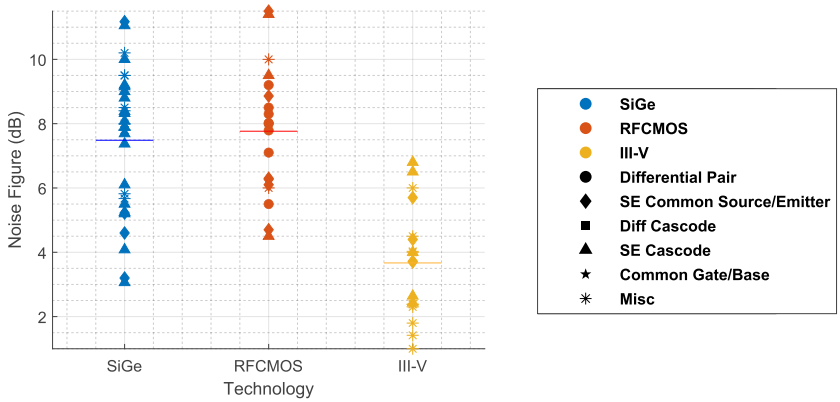

Figure 12. LNA: Noise Figure in the frequency range of 78.5–195 GHz. Horizontal lines represent mean values.

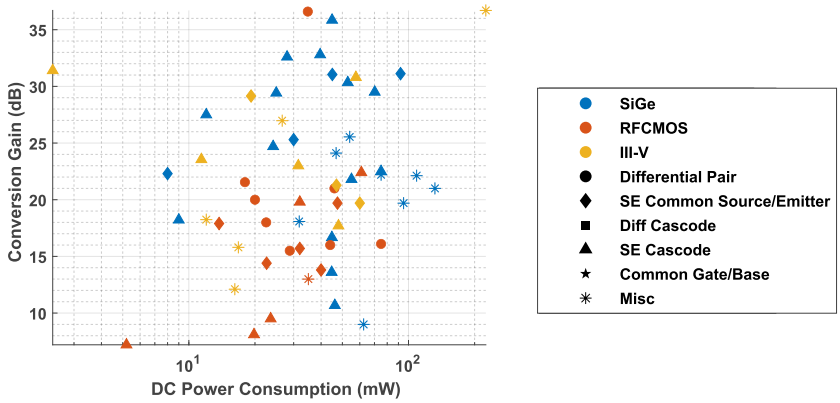

Figure 13. LNA: Conversion Gain over DC power consumption in the frequency range of 78.5–200 GHz.

Linearity is also of prime concern for LNAs because the systems dynamic range may be restricted as a result of intermodulation distortion (e.g., blocking or cross-modulation) [13]. Nevertheless, a lack of available data is apparent from Figure 14. This scarcity might be explained by low signal levels emerging from the free space loss (ct. Equation (1)) and the corresponding rarely arising need to measure it. EM-crosstalk resulting from a PA in close proximity, however, could occur, increasing the input power past the IP1dB. From the limited data, III–V semiconductors seem to be the least affected by those effects. Whether SiGe or RFCMOS devices possess better linearity, however, is not decisive due to the data shortage. Another statistical uncertainty is the higher linearity in differential devices in contrast to their single-ended equivalents.

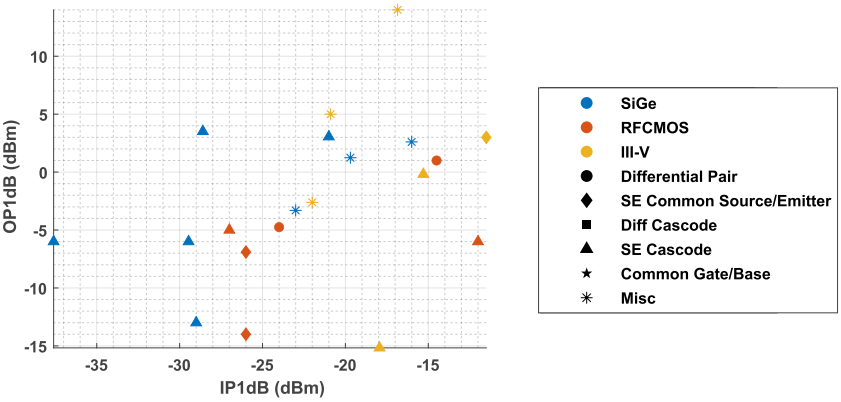

Figure 14. LNA: Linearity shown in OP1dB and IP1dB for a frequency range of 95–190 GHz.

2.5. Mixer

Frequency conversion is a method to decrease (downconvert) or increase (upconvert) the frequency of a signal by either transistor switching as is the case for gilbert cells or by using the transconductance of a nonlinear element such as diodes or transistors. Since only downconverters are conventionally employed in radar receive paths, they have been exclusively analyzed in this study. In downconverters, the received signal is applied to the RF-Port, the (frequency multiplied) VCO signal is connected to the LO-Port and the generally baseband frequency output is generated at the IF-Port. Yet, in the investigated publications, Mixers have been operated with varying IF-Frequencies, spanning from 1 MHz to 31 GHz ($\overline{\text{IF}} = 3.71$ GHz). This prevents a definitive comparison from being conducted as a consequence of the differing intensity of frequency dependent effects such as the 1/f-Noise. The results should thus be regarded with caution. As an element in the receiver chain, one of the most important characteristics of a mixer is its NF. The lowest average noise contribution, discerned from Figure 15, is $\overline{\text{NF}} = 10.43$ dB in III–V semiconductors. The different III–V semiconductor devices also achieve values in close proximity to each other, exemplifying the feasibility of this NF. Having competitive values with III–V semiconductors, SiGe has a high data spread that results in a worse mean NF with a value of 13.6 dB. Further investigations are required to give a conclusive statement about RFCMOS's noise performance. Disregarding the outlier with the worst Noise Figure, values similar to the other two technologies are attained. In this case, RFCMOS performs the best on average out of the three investigated technologies. With the outliers, however, the worst average NF is reported (14.91 dB).

Since the lack of data is also present in other categories such as the DC power consumption, the CG of the gathered mixers is separately shown in Figure 16. A comparable CG range is accomplished in all three technologies. The value distribution, however, distinguishes III–V semiconductors mixers as having the worst ($\overline{\text{CG}_{\text{III-V}}} = -6.12$ dB) and SiGe as having the best ($\overline{\text{CG}_{\text{SiGe}}} = 7.46$ dB) mean CG. RFCMOS, meanwhile, has a uniform dispersal of CGs ($\overline{\text{CG}_{\text{RFCMOS}}} = -3.4$ dB). This distribution might be connected to the utilization of buffer stages, in which case the CG would reflect on the performance of those buffer stages instead of the mixers.

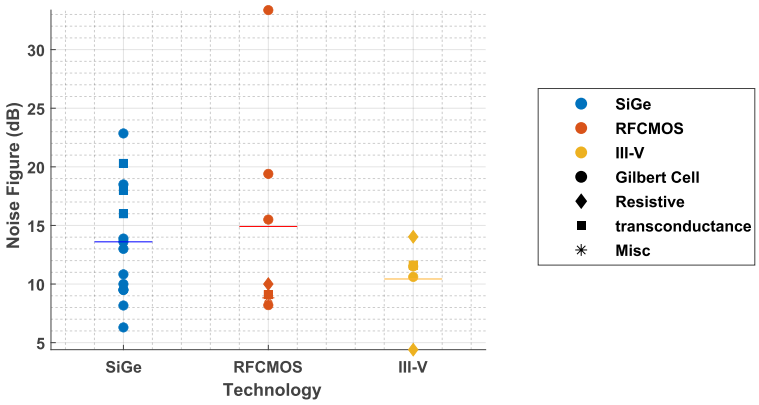

Figure 15. Mixer: Noise Figure in the frequency range of 90–200 GHz. Horizontal lines represent mean values.

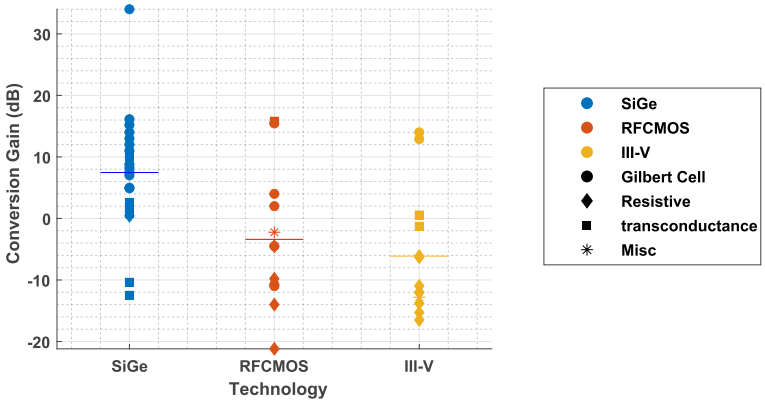

Figure 16. Mixer: Conversion Gain in the frequency range of 90–200 GHz. Horizontal lines represent mean values.

High LO-Powers typically facilitate an improved mixer operation. Depending on the LO-RF Isolation of the mixer, a significant amount of this power might be forwarded to the RF-Port, causing interference, disturbance or emission in the Rx. If an LNA is present, this effect can largely be neglected due to the LNA's high reverse isolation. However, without an LNA, the LO-RF Isolation becomes an important, rarely reported mixer parameter that can only be compared indecisively as Figure 17 demonstrates. The limited data show that the isolation is consistently high in RFCMOS, lower with a higher spread in SiGe, and it has a broad range with both low and high values in III–V semiconductors.

In regard to the mixer topologies, the most widespread architecture depends on the respective technology. Because of the modest $1/f$ noise performance in RFCMOS and III–V composites, the least amount of transistors should carry out the frequency conversion. Hence, resistive mixers and single-device transconductance mixers have become common. They additionally benefit from an increase in linearity, which is confirmed in the gathered data, with no discernable effect on the NF. Contrastingly, Gilbert cells or cascode transconductance mixers are usually seen in SiGe publications. While Gilbert mixers are known to typically demonstrate the highest Gains (cf. Figure 16), no improved Isolation in comparison to the other architectures could be verified [37,38].

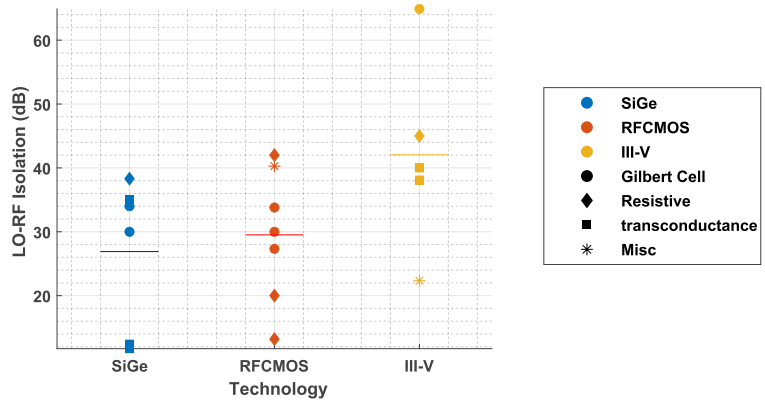

Figure 17. Mixer: LO-RF Isolation in the frequency range of 90–180 GHz. Horizontal lines represent mean values.

3. Conclusions

The three most commonly used technologies—RFCMOS, SiGe HBT and III–V semiconductor composites—have been investigated by means of a literature study. Insight was given into the most crucial radar circuit parameters, and the technologies were compared based upon them. Particularly, the low cost connected with the efficiency both in area and power consumption (cf. Figures 18 and 19) alongside the ease of baseband interfacing are

favorable traits in RFCMOS. Additionally, no substantial noise variation between RFCMOS and SiGe was determined. Yet, its high-frequency struggle with rather poor output power hampers its practicality. In stark contrast, III–V semiconductor devices excel at attaining the highest possible performance in single devices, but they are held back by high production costs, high area and power consumption as well as fewer fabrication facilities. Lastly, the usage of the widely established SiGe HBTs leads to a compromise between efficiency and performance, which is why it is the most common technology for D-Band radar systems.

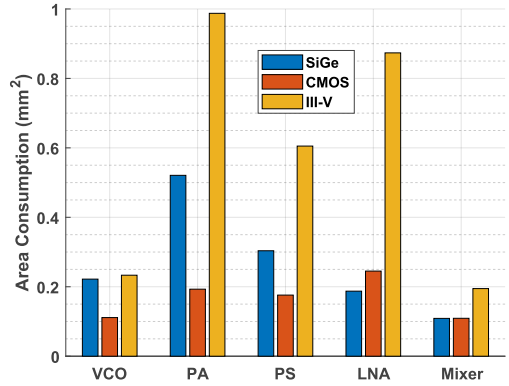

Figure 18. Average Area Consumption of all circuit elements.

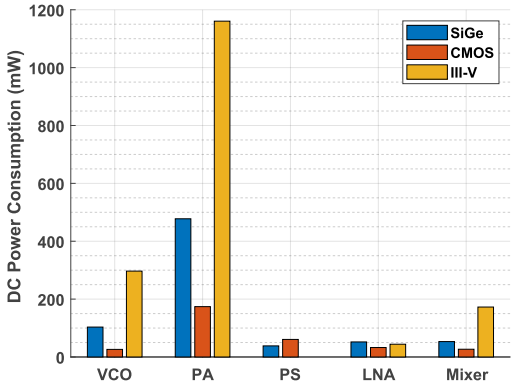

Figure 19. Average DC Power Consumption of all circuit elements.

4. Disclaimer

The authors are not liable for any inaccuracy or falsities connected with assuming, calculating and/or estimating values from the publications based on the given diagrams and data. The data were taken from the provided measurement plots whenever possible, and data non-conforming to the principles and comparison methods used in this study were adjusted accordingly. The authors are not accountable for any future use of this study.

Author Contributions: Conceptualization, N.P. and H.P.; methodology, P.S. and H.P.; software, P.S.; validation, H.P.; formal analysis, P.S.; investigation, P.S. and H.P.; resources, S.T.A.; data curation, P.S.; writing—original draft preparation, P.S.; writing—review and editing, P.S., H.P. and T.W.; visualization, P.S.; supervision, N.P.; project administration, S.T.A.; funding acquisition, N.P. All authors have read and agreed to the published version of the manuscript.

Funding: This research received no external funding

Institutional Review Board Statement: Not applicable.

Informed Consent Statement: Not applicable.

Data Availability Statement: The data will be made publically available at the website of the "Institute of Integrated Systems" (https://etit.ruhr-uni-bochum.de/insys/).

Acknowledgments: This literature study was carried out in accordance with the research project "automotive 140 GHz high resolution radar". We thank Huawei Technologies Duesseldorf GmbH for their support within the given research project.

Conflicts of Interest: The authors declare no conflict of interest.

References

1. Wallace, H.B. An application of advanced SiGe to millimeter-wave phased arrays. In Proceedings of the 2012 IEEE/MTT-S International Microwave Symposium Digest, 17.-22 June 2012, Montreal, QC, Canada; pp. 1–3. https://doi.org/10.1109/MWSYM.2012.6258285.
2. Romstadt, J.; Papurcu, H.; Zaben, A.; Hansen, S.; Aufinger, K.; Pohl, N. Comparison on spectral purity of two SiGe D-Band frequency octuplers in MIMO radar MMICs. In Proceedings of the 2021 IEEE BiCMOS and Compound Semiconductor Integrated Circuits and Technology Symposium (BCICTS), 05-08 December 2021, Monterey, CA, USA; pp. 1–4. https://doi.org/10.1109/BCICTS50416.2021.9682491.
3. Jaeschke, T.; Kueppers, S.; Pohl, N.; Barowski, J. Calibrated and Frequency Traceable D-Band FMCW Radar for VNA-like S-Parameter Measurements. In Proceedings of the 2022 IEEE Radio and Wireless Symposium (RWS), 16-19 January 2022, Las Vegas, NV, USA; pp. 64–67. https://doi.org/10.1109/RWS53089.2022.9719876.
4. Kueppers, S.; Jaeschke, T.; Pohl, N.; Barowski, J. Versatile 126–182 GHz UWB D-Band FMCW Radar for Industrial and Scientific Applications. *IEEE Sens. Lett.* **2022**, *6*, 1–4. https://doi.org/10.1109/LSENS.2021.3130709.
5. Appleby, R.; Anderton, R.N. Millimeter-Wave and Submillimeter-Wave Imaging for Security and Surveillance. *Proc. IEEE* **2007**, *95*, 1683–1690. https://doi.org/10.1109/JPROC.2007.898832.
6. Song, H.; Nagatsuma, T. Present and Future of Terahertz Communications. *IEEE Trans. Terahertz Sci. Technol.* **2011**, *1*, 256–263. https://doi.org/10.1109/TTHZ.2011.2159552.
7. Kurner, T. Towards Future THz Communications Systems. *Inter. J. Terahertz Sci. Technol.* **2012**, Vol.5, No.1: 11-17. http://www.tstnetwork.org/10.11906/TST.011-017.2012.03.02
8. Kucharski, M.; Ergintav, A.; Ahmad, W.A.; Krstić , M.; Ng, H.J.; Kissinger, D. A Scalable 79-GHz Radar Platform Based on Single-Channel Transceivers. *IEEE Microw. Wirel. Components Lett.* **2019**, *67*, 3882–3896. https://doi.org/10.1109/TMTT.2019.2914104.
9. Hasch, J.; Topak, E.; Schnabel, R.; Zwick, T.; Weigel, R.; Waldschmidt, C. Millimeter-Wave Technology for Automotive Radar Sensors in the 77 GHz Frequency Band. *IEEE Trans. Microw. Theory Tech.* **2012**, *60*, 845–860. https://doi.org/10.1109/TMTT.2011.2178427.
10. Wang, H.; Huang, Tz.; Mannem, N.S.; Lee, J.; Garay, E.; Munzer, D.; Liu, E.; Liu, Y.; Lin, B.; Eleraky, M.; et al. Power Amplifiers Performance Survey 2000-Present. Available online: https://gems.ece.gatech.edu/PA_survey.html (accessed on 27 April 2022).
11. Rimmelspacher, J. Integrated VCO Performance Survey. Available online: http://www.elektronik.ovgu.de/Rimmelspacher_VCO (accessed on 27 April 2022)
12. Voinigescu, S. *High-Frequency Integrated Circuits*; Cambridge University Press: Cambridge, UK, 2013.
13. Lee, T.H. *The Design of CMOS Radio-Frequency Integrated Circuits*; Cambridge University Press: Cambridge, UK, 2003.
14. Rogers, J.W.; Plett, C. *Radio Frequency Integrated Circuit Design*; Artech House: Norwood, MA, USA, 2010.
15. Kim, K.-J.; Lim, T.-H.; Park, H.-C.; Ahn, K.H. mm-Wave CMOS Colpitts VCO & Frequency divider for the 60GHz WPAN. In Proceedings of the 2009 IEEE 9th Malaysia International Conference on Communications (MICC), 15-17 December 2009, Kuala Lumpur, Malaysia; pp. 358–361. https://doi.org/10.1109/MICC.2009.5431530.
16. Zhao, Y.; Heinemann, B.; Pfeiffer, U.R. Fundamental mode colpitts VCOs at 115 and 165-GHz. In Proceedings of the 2011 IEEE Bipolar/BiCMOS Circuits and Technology Meeting, 9-11 October 2011, Atlanta, GA, USA; pp. 33–36. https://doi.org/10.1109/BCTM.2011.6082744.
17. Jeong, Y.; Choi, S.; Yang, K. A Sub-100 μW Ku-Band RTD VCO for Extremely Low Power Applications. *IEEE Microw. Wirel. Components Lett.* **2009**, *19*, 569–571. https://doi.org/10.1109/LMWC.2009.2027071.
18. Quadrelli, F.; Panazzolo, F.; Tiebout, M.; Padovan, F.; Bassi, M.; Bevilacqua, A. A 18.2–29.3 GHz Colpitts VCOs bank with -119.5 dBc/Hz Phase Noise at 1 MHz Offset for 5G Communications. In Proceedings of the 2019 IEEE Radio Frequency Integrated Circuits Symposium (RFIC), 2-4 June 2019, Boston, MA, USA; pp. 167–170. https://doi.org/10.1109/RFIC.2019.8701813.
19. Gu, Q.J.; Xu, Z.; Chang, M.-C.F. Two-Way Current-Combining W -Band Power Amplifier in 65-nm CMOS. *IEEE Trans. Microw. Theory Tech.* **2012**, *60*, 1365–1374. https://doi.org/10.1109/TMTT.2012.2187536.
20. Zhang, J.; Wu, T.; Nie, L.; Ma, S.; Chen Y.; Ren, J. A 120–150 GHz Power Amplifier in 28-nm CMOS Achieving 21.9-dB Gain and 11.8-dBm Psat for Sub-THz Imaging System. *IEEE Access*. **2021**, *9*, 74752-74762. https://doi.org/10.1109/ACCESS.2021.3080710.
21. Son, H.S.; Jang, T.H.; Kim, S.H.; Jung, K.P.; Kim, J.H.; Park, C.S. Pole-Controlled Wideband 120 GHz CMOS Power Amplifier for Wireless Chip-to-Chip Communication in 40-nm CMOS Process. *IEEE Trans. Circuits Syst. II Express Briefs* **2019**, *66*, 1351–1355. https://doi.org/10.1109/TCSII.2018.2880308.
22. Li, S.; Rebeiz, G.M. High Efficiency D-Band Multiway Power Combined Amplifiers With 17.5–19-dBm Psat and 14.2–12.1% Peak PAE in 45-nm CMOS RFSOI. *IEEE J. Solid-State Circuits*, **2022**, *57*, 1332–1343. https://doi.org/10.1109/JSSC.2022.3145394.

23. Park, D.-W.; Utomo, D.R.; Yun, B.; Mahmood, H.U.; Lee, S.-G. A D-Band Power Amplifier in 65-nm CMOS by Adopting Simultaneous Output Power-and Gain-Matched Gmax-Core. *IEEE Access* **2021**, *9*, 99039–99049. https://doi.org/10.1109/ACCESS.2021.3096423.
24. Su, G.; Wan, C.; Chen, D.; Gao, X.; Sun, L. A 129.5–151.5GHz Fully Differential Power Amplifier in 65nm CMOS. In Proceedings of the 2019 IEEE MTT-S International Wireless Symposium (IWS), 19-22 May 2019, Guangzhou, China; pp. 1–3. https://doi.org/10.1109/IEEE-IWS.2019.8803888.
25. Kucharski, M.; Borngräber, J.; Wang, D.; Kissinger, D.; Ng, H.J. A 109–137 GHz power amplifier in SiGe BiCMOS with 16.5 dBm output power and 12.8% PAE. In Proceedings of the 2017 47th European Microwave Conference (EuMC), 10-12 October 2017, Nuremberg, Germany; pp. 1021–1024. https://doi.org/10.23919/EuMC.2017.8231020.
26. Al-Eryani, J.; Knapp, H.; Wursthorn, J.; Aufinger, K., Majied, S.; Li, H.; Boguth, S.; Lachner, R.; Böck, J.; Maurer, L. A 162 GHz power amplifier with 14 dBm output power. 2016 IEEE Bipolar/BiCMOS Circuits and Technology Meeting (BCTM), 2016; pp. 174–177. https://doi.org/10.1109/BCTM.2016.7738965.
27. Sene, B.; Knapp, H.; Li, H.; Kammerer, J.; Majied, S.; Aufinger, K.; Fritzin, J.; Reiter, D.; Pohl, N. A 16-dBm D-Band Power Amplifier with a Cascaded CE and CB Output Power Stage Using a Stub Matching Topology. In Proceedings of the 2019 IEEE BiCMOS and Compound semiconductor Integrated Circuits and Technology Symposium (BCICTS), 3-6 November 2019, Nashville, TN, USA; pp. 1–4. https://doi.org/10.1109/BCICTS45179.2019.8972772.
28. Ahmed, F.; Furqan, M.; Aufinger, K.; Stelzer, A. A SiGe-based broadband 100–180-GHz differential power amplifier with 11 dBm peak output power and >1.3THz GBW. In Proceedings of the 2016 11th European Microwave Integrated Circuits Conference (EuMIC), 3-4 October 2016, London, UK; pp. 257–260. https://doi.org/10.1109/EuMIC.2016.7777539.
29. Zhao, D.; Reynaert, P. *CMOS 60-GHz and E-band Power Amplifiers and Transmitters*; Springer: Berlin, Germany, 2015.
30. Ma, Z.; Jiang, N. On the operation configuration of SiGe HBTs based on power gain analysis. *IEEE Trans. Electron Devices* **2005**, *52*, 248–255. https://doi.org/10.1109/TED.2004.842541.
31. Pepe, D.; Zito, D. Two mm-wave vector modulator active phase shifters with novel iq generator in 28 nm fdsoi cmos. *IEEE J. Solid-State Circuits* **2016**, *52*, 344–356. https://doi.org/10.1109/JSSC.2016.2605659.
32. Afroz, S.; Koh, K.-J. W-band (92–100 ghz) phased-array receive channel with quadrature -hybrid-based vector modulator. *IEEE Trans. Circuits Syst. I Regul. Pap.* **2018**, *65*, 2070–2082.
33. Parveg, D.; Varonen, M.; Karaca, D.; Vahdati, A.; Kantanen, M.; Halonen, K.A.I. Design of a D-Band CMOS Amplifier Utilizing Coupled Slow-Wave Coplanar Waveguides. *IEEE Microw. Wirel. Components Lett.* **2018**, *66*, 1359–1373. https://doi.org/10.1109/TMTT.2017.2777976.
34. Weber, R.; Massler, H.; Leuther, A. D-band low-noise amplifier MMIC with 50 % bandwidth and 3.0 dB noise figure in 100 nm and 50 nm mHEMT technology. In Proceeding of the 2017 IEEE MTT-S International Microwave Symposium (IMS), 4-9 June 2017, Honolulu, HI, USA; pp. 756–759. https://doi.org/10.1109/MWSYM.2017.8058686.
35. Zhang, Y.; Liang, W.; Esposito, C.; Jin, X.; Sakalas, P.; Schröter, M. LO Chain (×12) Integrated 190-GHz Low-Power SiGe Receiver With 49-dB Conversion Gain and 171-mW DC Power Consumption. *IEEE Microw. Wirel. Components Lett.* **2021**, *69*, 1943–1954. https://doi.org/10.1109/TMTT.2020.3044095.
36. Yishay, R.B.; Shumaker, E.; Elad, D. A 122–150 GHz LNA with 30 dB gain and 6.2 dB noise figure in SiGe BiCMOS technology. In Proceeding of the 2015 IEEE 15th Topical Meeting on Silicon Monolithic Integrated Circuits in RF Systems, 26-28 January 2015, San Diego, CA, USA; pp. 15–17. https://doi.org/10.1109/SIRF.2015.7119860.
37. Deng, X.-D.; Li, Y.; Wu, W.; Xiong, Y.-Z. D-band down conversion chipset with I-Q outputs using 0.13μm SiGe BiCMOS technology. In Proceeding of the 2015 IEEE 11th International Conference on ASIC (ASICON), 3-6 November 2015, Chengdu, China; pp. 1–4. https://doi.org/10.1109/ASICON.2015.7516977.
38. Shiba, S.;Sato, M.; Matsumura, H.; Kawano, Y.; Takahashi, T.; Suzuki, T.; Nakasha, Y.; Iwai, T.; Hara, N. An F-band mixer module with a built-in broadband IF amplifier for spectrum analysis with low intermodulation distortion. In Proceeding of the 2014 IEEE International Microwave and RF Conference (IMaRC), 15-17 December 2014, Bangalore, India; pp. 270–273. https://doi.org/10.1109/IMaRC.2014.7039025.
39. Lee, J.; Moon, Y. A design of low power 70GHz CMOS VCO for wireless communication system. In Proceedings of the 2014 IEEE International Conference on Electron Devices and Solid-State Circuits, 18-20 June 2014, Chengdu, Sichuan, China; pp. 1–2. https://doi.org/10.1109/EDSSC.2014.7061164.
40. Chai, S.W.; Yang, J.; Ku, B.; Hong, S. Millimeter wave CMOS VCO with a high impedance LC tank. In Proceedings of the 2010 IEEE Radio Frequency Integrated Circuits Symposium, 23-25 May 2010, Anaheim, CA, USA; pp. 545–548. https://doi.org/10.1109/RFIC.2010.5477380.
41. Mansour, I.; Mansour, M.; Aboualalaa M.; Allam, A.; Abdel-Rahman, A.B.; Abo-Zahhad, M.; Pokharel, R.K. 70 % Improvement in Q-Factor of Spiral Inductor and its Application in Switched K-Band VCO Using 0.18 μM CMOS Technology. In Proceedings of the 2018 Asia-Pacific Microwave Conference (APMC), 6-9 November 2018, Kyoto, Japan; pp. 1133–1135. https://doi.org/10.23919/APMC.2018.8617138.
42. Miyashita, K. A 1.0V 31GHz differentially controlled CMOS VCO with 191.9 dBc/Hz FOM. In Proceedings of the 2012 IEEE/MTT-S International Microwave Symposium Digest, 17-22 June 2012, Montreal, QC, Canada; pp. 1–3. https://doi.org/10.1109/MWSYM.2012.6257762.

43. Jahan, N.; Barakat, A.; Pokharel, R.K. A -192.7-dBc/Hz FoM K_U -Band VCO Using a DGS Resonator With a High-Band Transmission Pole in 0.18- μm CMOS Technology. *IEEE Microw. Wirel. Components Lett.* **2019**, *29*, 814–817. https://doi.org/10.1109/LMWC.2019.2950525.
44. Wang, T. A K-Band Low-Power Colpitts VCO With Voltage-to-Current Positive-Feedback Network in 0.18 μm CMOS. *IEEE Microw. Wirel. Components Lett.* **2011**, *21*, 218–220. https://doi.org/10.1109/LMWC.2011.2108275.
45. Kuo, Y.; Tsai, J.; Huang, T.; Wang, H. A V-band VCO using fT-doubling technique in 0.18-μm CMOS. In Proceedings of the Asia-Pacific Microwave Conference 2011, 5-8 December 2011, Melbourne, VIC, Australia; pp. 251–254.
46. Jahan, N.; Baichuan, C.; Pokharel, R.K.; Barakat, A. A K-Band VCO Employing High Active Q-factor Defected Ground Structure Resonator in 0.18pm CMOS Technology. In Proceedings of the 2018 IEEE International Symposium on Circuits and Systems (ISCAS), 27-30 May 2018, Florence, Italy; pp. 1–5. https://doi.org/10.1109/ISCAS.2018.8351670.
47. Zandieh, A.; Bonen, S.; Dadash, M.S.; Gong, M.J.; Hasch, J.; Voinigescu, S.P. 155 GHz FMCW and Stepped-Frequency Carrier OFDM Radar Sensor Transceiver IC Featuring a PLL With $<$30 ns Settling Time and 40 fs rms Jitter. *IEEE Trans. Microw. Theory Tech.* **2021**, *69*, 4908–4924. https://doi.org/10.1109/TMTT.2021.3094189.
48. Dadash, M.S.; Bonen, S.; Alakusu, U.; Harame, D.; Voinigescu, S.P. DC-170 GHz Characterization of 22nm FDSOI Technology for Radar Sensor Applications. In Proceedings of the 2018 13th European Microwave Integrated Circuits Conference (EuMIC), 23-25 September 2018, Madrid, Spain; pp. 158–161. https://doi.org/10.23919/EuMIC.2018.8539934.
49. Reiter, D.; Li, H.; Knapp, H.;Kammere, J.; Majied, S.; Sene, B.; Pohl,N. Low Phase Noise, Wide Tuning Range 20GHz Magnetic-Coupled Hartley-VCO in a 28nm CMOS Technology. In Proceedings of the 2019 IEEE Radio and Wireless Symposium (RWS), 20-23 January 2019, Orlando, FL, USA; pp. 1–3. https://doi.org/10.1109/RWS.2019.8714258.
50. Rimmelspacher, J.; Weigel, R.; Hagelauer, A.; Issakov, V. 30 % Frequency-tuning-range 60 GHz push-push VCO in 28 nm bulk CMOS technology. In Proceedings of the 2018 IEEE 18th Topical Meeting on Silicon Monolithic Integrated Circuits in RF Systems (SiRF), 14-17 January 2018, Anaheim, CA, USA; pp. 30–32. https://doi.org/10.1109/SIRF.2018.8304221.
51. Ding, X.; Yu, H.; Yu, B.; Xu, Z.; Gu, Q.J. A Superharmonic Injection based G-band Quadrature VCO in CMOS. In Proceedings of the 2020 IEEE/MTT-S International Microwave Symposium (IMS), 4-6 August 2020, Los Angeles, CA, USA; pp. 345–348. https://doi.org/10.1109/IMS30576.2020.9223816.
52. Chang, Y.-T.; Lu, H.-C. A D-band wide tuning range VCO using switching transformer. In Proceedings of the 2017 IEEE MTT-S International Microwave Symposium (IMS), 04-09 June 2017, Honololu, HI, USA; pp. 1353–1355. https://doi.org/10.1109/MWSYM.2017.8058864.
53. Liu, Y.; Mao, L.; Xie, S.; Chi, B. A 190 GHz VCO with Transformer-Based Push–Push Frequency Doubler in 40 nm CMOS. *Circuits Syst. Signal Process* **2019**, *38*, 425–444. https://doi.org/10.1007/s00034-018-0842-4
54. Katz, A.; Degani, O.; Shacham-Diamand, Y.; Socher, E. A beyond 60GHz cross-coupled fundamental VCO in 45nm CMOS. In Proceedings of the 2009 IEEE International Conference on Microwaves, Communications, Antennas and Electronics Systems, 9-11 November 2009, Tel Aviv, Israel; pp. 1–5. https://doi.org/10.1109/COMCAS.2009.5386021.
55. Rimmelspacher, J.; Weigel, R.; Hagelauer, A.; Issakov, V. LC Tank Differential Inductor-Coupled Dual-Core 60 GHz Push-Push VCO in 45 nm RF-SOI CMOS Technology. In Proceedings of the 2019 IEEE 19th Topical Meeting on Silicon Monolithic Integrated Circuits in RF Systems (SiRF), 20-23 January 2019, Orlando, FL, USA; pp. 1–3. https://doi.org/10.1109/SIRF.2019.8709120.
56. Rimmelspacher, J.; Weigel, R.; Issakov, V. Transformer-Coupled Octa-Core 60 GHz Push-Push VCO in a 45-nm RF-SOI CMOS Technology. In Proceedings of the 2019 IEEE International Conference on Microwaves, Antennas, Communications and Electronic Systems (COMCAS), 4-6 November 2019, Tel-Aviv, Israel; pp. 1–4. https://doi.org/10.1109/COMCAS44984.2019.8958108.
57. Volkaerts, W.; Steyaert, M.; Reynaert, P. A 120GHz quadrature frequency generator with 16.2GHz tuning range in 45nm CMOS. In Proceedings of the 2013 IEEE Radio Frequency Integrated Circuits Symposium (RFIC), 2-4 June 2013, Seattle, WA, USA; pp. 207–210. https://doi.org/10.1109/RFIC.2013.6569562.
58. Xu, X.; Chen, C.; Sugiura, T.; Yoshimasu, T. 18-GHz band low-power LC VCO IC using LC bias circuit in 56-nm SOI CMOS. In Proceedings of the 2017 IEEE Asia Pacific Microwave Conference (APMC), 13-16 November 2017, Kuala Lumpur, Malaysia; pp. 938–941. https://doi.org/10.1109/APMC.2017.8251604.
59. Trivedi, V.P.; To, K. A novel mmWave CMOS VCO with an AC-coupled LC tank. In Proceedings of the 2012 IEEE Radio Frequency Integrated Circuits Symposium, 17-19 June 2012, Montreal, QC, Canada; pp. 515–518. https://doi.org/10.1109/RFIC.2012.6242335.
60. Tan, W.; Wu, T.; Xing, Z.; Peng, Y.; Liu, H.; Kang, K. A 21.95–24.25 GHz Class-C VCO for 24 GHz FMCW Radar Applications. In Proceedings of the 2019 IEEE MTT-S International Wireless Symposium (IWS), 19-22 May 2019, Guangzhou, China; pp. 1–3. https://doi.org/10.1109/IEEE-IWS.2019.8804153.
61. Lee, C.J.; Kang, D.M.; Kim, J.H.; Byeon, C.W.; Park, C.S. A 110–125 GHz 27.5 dB Gain Low-power I/Q Receiver Front-end in 65 nm CMOS Technology. In Proceedings of the 2018 IEEE/MTT-S International Microwave Symposium - IMS, 10-15 June 2018, Philadelphia, PA, USA; pp. 599–602. https://doi.org/10.1109/MWSYM.2018.8439204.
62. Holisaz, H.; Safavi-Naeini, S. A Low Noise D-Band VCO With a Wide Bandwidth and a Steady Output Power. *IEEE Microw. Wirel. Components Lett.* **2015**, *25*, 742–744. https://doi.org/10.1109/LMWC.2015.2481083.
63. Khamaisi, B.; Socher, E. A 159–169 GHz frequency source with 1.26 mW peak output power in 65 nm CMOS. In Proceedings of the 2013 European Microwave Conference, 6-10 October 2013, Nuremberg, Germany; pp. 1507–1510. https://doi.org/10.23919/EuMC.2013.6686955.

64. Volkaerts, W.; Steyaert, M.; Reynaert, P. 118GHz fundamental VCO with 7.8% tuning range in 65nm CMOS. In Proceedings of the 2011 IEEE Radio Frequency Integrated Circuits Symposium, 5-7 June 2011, Baltimore, MD, USA; pp. 1–4. https://doi.org/10.1109/RFIC.2011.5940642.
65. Otsuki, Y.; Yamazaki, D.; Khanh, M.; Iizuka, T. A 140 GHz area-and-power-efficient VCO using frequency doubler in 65nm CMOS. *IEICE Electron. Express* **2019**, *16*, 20190051. https://doi.org/16. 10.1587/elex.16.20190051.
66. Yi, X.; Liang, Z.; Feng, G.; Boon, C.C.; Meng, F. A 93.4-to-104.8 GHz 57 mW fractional-N cascaded sub-sampling PLL with true in-phase injection-coupled QVCO in 65 nm CMOS. In Proceedings of the 2016 IEEE Radio Frequency Integrated Circuits Symposium (RFIC), 22-24 May 2016, San Francisco, CA, USA; pp. 122–125. https://doi.org/10.1109/RFIC.2016.7508266.
67. Jeong, C.-H.; Kwon, C.; Park, S.-C.; Kim, S.-W. Design of push-push voltage-controlled oscillator for D-band applications. In Proceedings of the 2014 IEEE International Conference on Ultra-WideBand (ICUWB), 01-03 September 2014, Paris, France; pp. 327–330. https://doi.org/10.1109/ICUWB.2014.6959001.
68. Badalawa, W.; Lim, S.; Fujishima, M. 115GHz CMOS VCO with 4.4% tuning range. In Proceedings of the 2009 European Microwave Integrated Circuits Conference (EuMIC), 28-29 September 2009, Rome, Italy; pp. 128–131.
69. Xu, Z.; Gu, Q.j.; Wu, Y.-C.; Tang, A.; Lin,Y.-L; Chen, H.-H; Jou, C.; Chang, M.-C.F; D-band CMOS transmitter and receiver for multi-giga-bit/sec wireless data link. In Proceedings of the IEEE Custom Integrated Circuits Conference 2010, 19-22 September 2010, San Jose, CA; pp. 1–4. https://doi.org/10.1109/CICC.2010.5617617.
70. Ono, N.; Motoyoshi, M.; Katayama, K.; Fujishima, M. 125 GHz CMOS oscillator controlled by p-type bulk voltage. In Proceedings of the 2012 IEEE Radio and Wireless Symposium, 15-18 January 2012, Santa Clara, CA, USA; pp. 215–218. https://doi.org/10.1109/RWS.2012.6175387.
71. Kang, D.; Lee, C.J.; Son, H.S.; Lee, H.; Park, C.S. A 117 GHz all-parallel sub-harmonically Injection-Locked quadrature CMOS voltage-controlled oscillator. In Proceedings of the 2016 URSI Asia-Pacific Radio Science Conference (URSI AP-RASC), 21-25 August 2016, Seoul, Korea (South); pp. 647–649. https://doi.org/10.1109/URSIAP-RASC.2016.7601305.
72. Koo, H.; Kim, C.; Hong, S. A G-Band Standing-Wave Push–Push VCO Using a Transmission-Line Resonator. *IEEE Trans. Microw. Theory Tech.* **2015**, *63*, 1036–1045. https://doi.org/10.1109/TMTT.2015.2398445.
73. Siriburanon, T.; Ueno, T.; Kimura, K.; Kondo, S.; Deng, W.; Okada, K.; Matsuzawa, A. A 60-GHz sub-sampling frequency synthesizer using sub-harmonic injection-locked quadrature oscillators. In Proceedings of the 2014 IEEE Radio Frequency Integrated Circuits Symposium, 01-03 June 2014, Tampa, FL, USA; pp. 105–108. https://doi.org/10.1109/RFIC.2014.6851670.
74. Laskin, E.; Khanpour, M.; Aroca, R.; Tang, K.W.; Garcia, P.; Voinigescu, S.P. A 95GHz Receiver with Fundamental-Frequency VCO and Static Frequency Divider in 65nm Digital CMOS. In Proceedings of the 2008 IEEE International Solid-State Circuits Conference - Digest of Technical Papers, 03-07 February 2008, San Francisco, CA, USA; pp. 180–605. https://doi.org/10.1109/ISSCC.2008.4523116.
75. Liu, G.; Berenguer, R.; Xu, Y. A MM-Wave Configurable VCO Using MCPW-Based Tunable Inductor in 65-nm CMOS. *IEEE Trans. Circuits Syst. II Express Briefs* **2011**, *58*, 842–846. https://doi.org/10.1109/TCSII.2011.2172718.
76. Kim, D. D.; Kim, J.; Plouchart, J. O.; Cho, C.; Li, W.; Lim, D.; Trzcinski, R.; Kumar, M.; Norris, C.; Ahlgren, D. A 70GHz Manufacturable Complementary LC-VCO with 6.14GHz Tuning Range in 65nm SOI CMOS. In Proceedings of the 2007 IEEE International Solid-State Circuits Conference. Digest of Technical Papers, 11-15 February 2007, San Francisco, CA, USA; pp. 540–620. https://doi.org/10.1109/ISSCC.2007.373533.
77. Yin, J.; Luong, H.C. A 57.5–90.1-GHz Magnetically Tuned Multimode CMOS VCO. *IEEE J. Solid-State Circuits* **2013**, *48*, 1851–1861. https://doi.org/10.1109/JSSC.2013.2258796.
78. Li, W.; Cheng, J.; Wu, Y.; Huang, T. A 23.67-to-45-GHz wide tuning range dual VCO with phase noise enhancement in 90-nm CMOS technology. In Proceedings of the 2013 IEEE MTT-S International Microwave Symposium Digest (MTT), 2-7 June 2013, Seattle, WA, USA; pp. 1–3. https://doi.org/10.1109/MWSYM.2013.6697478.
79. Huang, Z. A 57.15–59.00GHz CMOS LC-VCO for V-Band high speed WPAN communication system. In Proceedings of the 2011 41st European Microwave Conference, 10-13 October 2011, Manchester, UK; pp. 671–673. https://doi.org/10.23919/EuMC.2011.6101773.
80. Katz, A.; Degani, O.; Socher, E. Design and optimization of a low-noise cross-coupled fundamental VCO in 90nm CMOS for 60GHz applications. In Proceedings of the 2011 IEEE 11th Topical Meeting on Silicon Monolithic Integrated Circuits in RF Systems, 17-19 January 2011, Glendale, AZ, USA; pp. 13–16. https://doi.org/10.1109/SIRF.2011.5719316.
81. Akhter, N.; Amin, M.T.; Faruqe, O. A High Figure of Merit Low Power LC VCO for D Band Applications. In Proceedings of the 2019 22nd International Conference on Computer and Information Technology (ICCIT), 18-20 December 2019, Dhaka, Bangladesh; pp. 1–6. https://doi.org/10.1109/ICCIT48885.2019.9038428.
82. Lin, Y.; Lan, K.; Lin, Y.; Chuang, M. 94 GHz VCO using negative capacitance technique. In Proceedings of the 2017 USNC-URSI Radio Science Meeting (Joint with AP-S Symposium), 9-14 July 2017, San Diego, CA, USA; pp. 39–40. https://doi.org/10.1109/USNC-URSI.2017.8074886.
83. Cao, C.; O, K.K. A 140-GHz fundamental mode voltage-controlled oscillator in 90-nm CMOS technology. *IEEE Microw. Wirel. Components Lett.* **2006**, *16*, 555–557. https://doi.org/10.1109/LMWC.2006.882385.
84. Lin, Y.-S.; Lan, K.-S.; Lin, Y.-C.; Lin, Y.-W. 95/190 GHz push-push VCO in 90 nm CMOS. In Proceedings of the 2017 USNC-URSI Radio Science Meeting (Joint with AP-S Symposium), 9-14 July 2017, San Diego, CA, USA; pp. 37–38. https://doi.org/10.1109/USNC-URSI.2017.8074885.

85. Chang, H.; Wang, H. A 98/196 GHz Low Phase Noise Voltage Controlled Oscillator With a Mode Selector Using a 90 nm CMOS Process. *IEEE Microw. Wirel. Components Lett.* **2009**, *19*, 170–172. https://doi.org/10.1109/LMWC.2009.2013742.
86. Lin, K.-T.; Chen, H.-K.; Lu, S.-S. 100 GHz transformer-coupled quadrature oscillator. *Electron. Lett.* **2013**, *49*, 266–267. https://doi.org/10.1049/el.2012.3492.
87. Lee, J.; Liu, M.; Wang, H. A 75-GHz Phase-Locked Loop in 90-nm CMOS Technology. *IEEE J. Solid-State Circuits* **2008**, *43*, 1414–1426. https://doi.org/10.1109/JSSC.2008.922719.
88. Chu, S.; Wang, C. An 80 GHz Wide Tuning Range Push-Push VCO With gm-Boosted Full-Wave Rectification Technique in 90 nm CMOS. *IEEE Microw. Wirel. Components Lett.* **2012**, *22*, 203–205. https://doi.org/10.1109/LMWC.2012.2189377.
89. Kim, D.; Jeon, S. W- and G-Band GaN Voltage-Controlled Oscillators With High Output Power and High Efficiency. *IEEE Microw. Wirel. Components Lett.* **2021**, *69*, 3908–3916. https://doi.org/10.1109/TMTT.2021.3092362.
90. Kozhuharov, R.; Bao, M.; Gavell, M.; Zirath, H. A W- and G-band MMIC source using InP HBT technology. In Proceedings of the 2012 IEEE/MTT-S International Microwave Symposium Digest, 17-22 June 2012, Montreal, QC, Canada; pp. 1–3. https://doi.org/10.1109/MWSYM.2012.6258435.
91. Zhang, L.; Pullela, R.; Winczewski, C.; Chow, J.; Mensa, D.; Jaganathan, S.; Yu, R. A 37/spl sim/50 GHz InP HBT VCO IC for OC-768 fiber optic communication applications. In Proceedings of the 2002 IEEE Radio Frequency Integrated Circuits (RFIC) Symposium. Digest of Papers (Cat. No.02CH37280), 3-4 June 2002, Seattle, WA, USA; pp. 85–88. https://doi.org/10.1109/RFIC.2002.1011929.
92. Jeong, Y.; Choi, S.; Yang, K. Low power K-band second harmonic balanced VCO IC using InP based RTDs. In Proceedings of the 2010 22nd International Conference on Indium Phosphide and Related Materials (IPRM), 31 May - 4 June 2010, Takamatsu, Japan; pp. 1–3. https://doi.org/10.1109/ICIPRM.2010.5516373.
93. Lin, R.; Liu, J.; Su, G.; Jiang, W. A 140 GHz common-base cross-coupled VCO with feedback inductor in InP HBT technology. In Proceedings of the 2017 Sixth Asia-Pacific Conference on Antennas and Propagation (APCAP), 16-19 October 2017, Xi'an, China; pp. 1–3. https://doi.org/10.1109/APCAP.2017.8420674.
94. Lao, Z.; Jensen, J.; Guinn, K.; Sokolich, M. 80-GHz differential VCO in InP SHBTs. *IEEE Microw. Wirel. Components Lett.* **2004**, *14*, 407–409. https://doi.org/10.1109/LMWC.2004.832056.
95. Kobayashi, K. W.; Oki, A. K.; Tran, L. T.; Cowles, J. C.; Gutierrez-Aitken, A.; Yamada, F.; Block,T. R.; Streit, D. C. A 108-GHz InP-HBT monolithic push-push VCO with low phase noise and wide tuning bandwidth. *IEEE J. Solid-State Circuits* **1999**, *34*, 1225–1232. https://doi.org/10.1109/4.782080.
96. Baeyens, Y.; Dorschky, C.; Weimann, N.; Lee, Q.; Kopf, R.; Georgiou, G.; MAttia, J. P.; Hamm, R.; Chen, Y. K. Compact InP-based HBT VCOs with a wide tuning range at W- and D-band. *IEEE Microw. Wirel. Components Lett.* **2000**, *48*, 2403–2408. https://doi.org/10.1109/22.898990.
97. Li, Z.; Liu, J.; Qiu, Z.; Su, G.; Sun, L. A 95.5–101 GHz Voltage Control Oscillator in 0.13 μm InP HBT. In Proceedings of the 2018 IEEE Asia-Pacific Conference on Antennas and Propagation (APCAP), 5-8 August 2018, Auckland, New Zealand; pp. 367–369. https://doi.org/10.1109/APCAP.2018.8538142.
98. Choi, S.; Jeong, Y.; Yang, K. 14 GHz InP-based RTD MMIC VCOs with Ultra Low DC Power Consumption. In Proceedings of the 2006 International Conference on Indium Phosphide and Related Materials Conference Proceedings, 8-11 May 2006, Princeton, NJ, USA; pp. 439–441. https://doi.org/10.1109/ICIPRM.2006.1634211.
99. Lai, S.; Kuylenstierna, D.; Kozhuharov, R.; Hansson, B.; Zirath, H. An LC VCO for High Power Millimeter-Wave Signal Generation. In Proceedings of the 2013 IEEE Compound Semiconductor Integrated Circuit Symposium (CSICS), 13-16 October 2013, Monterey, CA, USA; pp. 1–4. https://doi.org/10.1109/CSICS.2013.6659216.
100. Stuenkel, M.; Feng, M. An InP VCO with Static Frequency Divider for Millimeter Wave Clock Generation. In Proceedings of the 2010 IEEE Compound Semiconductor Integrated Circuit Symposium (CSICS), 3-6 October 2010, Monterey, CA, USA; pp. 1–4. https://doi.org/10.1109/CSICS.2010.5619658.
101. Djahanshahi, H.; Saniei, N.; Voinigescu, S.P.; Malikpaard, M.C.; Salama, C.A.T. A 20-GHz InP-HBT voltage-controlled oscillator with wide frequency tuning range. *IEEE Microw. Wirel. Components Lett.* **2001**, *49*, 1566–1572. https://doi.org/10.1109/22.942568.
102. Yu, M.; Ward, R.J.; Newgard, R.A.; Urteaga, M. A compact 43-GHz monolithic differential VCO in 0.5-μm InP DHBT technology. *IEEE Microw. Wirel. Components Lett.* **2006**, *16*, 281–283. https://doi.org/10.1109/LMWC.2006.873499.
103. Withitsoonthorn, S.; Blayac, S.; Riet, M.; Berdaguer, P.; Gonzalez, C. A 48 GHz Fully Integrated Differential VCO in InP DHBT Technology. In Proceedings of the 2003 33rd European Microwave Conference, 7 October 2003, Munich, Germany; pp. 571–574. https://doi.org/10.1109/EUMA.2003.341017.
104. Makon, R.; Driad, R.; Schneider, K.; Aidam, R.; Schlechtweg, M.; Weimann, G. Fundamental W-Band InP DHBT-Based VCOs With Low Phase Noise and Wide Tuning Range. In Proceedings of the 2007 IEEE/MTT-S International Microwave Symposium, 3-8 June 2007, Honolulu, HI, USA; pp. 649–652. https://doi.org/10.1109/MWSYM.2007.379985.
105. Kurdoghlian, A.; Mokhtari, M.; Fields, C.H.; Thomas, S. 44 GHz fully integrated and differential monolithic VCOs with wide tuning range in AlInAs/InGaAs/InP DHBT. In Proceedings of the 24th Annual Technical Digest Gallium Arsenide Integrated Circuit (GaAs IC) Symposiu, 20-23 October 2002, Monterey, CA, USA; pp. 287–290. https://doi.org/10.1109/GAAS.2002.1049079.
106. Makon, R. E.; Schneider, K.; Driad, R.; Lang, M.; Aidam, R.; Quay, R.; Weimann, G. Fundamental low phase noise InP-based DHBT VCOs with high output power operating up to 75 GHz.*IEEE Compd. Semicond. Integr. Circuit Symp.* **2004**, *2004*, 159–162. https://doi.org/10.1109/CSICS.2004.1392521.

107. Barghouthi, A.; Ellinger, F. Design of a 54 to 63 GHz differential common collector SiGe Colpitts VCO. In Proceedings of the 18-th INTERNATIONAL CONFERENCE ON MICROWAVES, RADAR AND WIRELESS COMMUNICATIONS, 14-16 June 2010, Vilnius, Lithuania; pp. 1–4.
108. Jahn, M.; Aufinger, K.; Meister, T.F.; Stelzer, A. 125 to 181 GHz fundamental-wave VCO chips in SiGe technology. In Proceedings of the 2012 IEEE Radio Frequency Integrated Circuits Symposium, 17-19 June 2012, Montreal, QC, Canada; pp. 87–90. https://doi.org/10.1109/RFIC.2012.6242238.
109. Pfeiffer, U.R.; Öjefors, E.; Zhao, Y. A SiGe quadrature transmitter and receiver chipset for emerging high-frequency applications at 160GHz. In Proceedings of the 2010 IEEE International Solid-State Circuits Conference - (ISSCC), 7-11 February 2010, San Francisco, CA, USA; pp. 416–417. https://doi.org/10.1109/ISSCC.2010.5433832.
110. Balteanu, A.; Sarkas, I.; Adinolfi, V.; Dacquay, E.; Tomkins, A.; Celi, D.; Chevalier, P.; Voinigescu, S. P. Characterization of a 400-GHz SiGe HBT technology for low-power D-Band transceiver applications. In Proceedings of the 2012 IEEE/MTT-S International Microwave Symposium Digest, 17-22 June 2012, Montreal, QC, Canada; pp. 1–3. https://doi.org/10.1109/MWSYM.2012.6259705.
111. Muralidharan, S.; Wu, K.; Hella, M. A 110–132GHz VCO with 1.5dBm peak output power and 18.2% tuning range in 130nm SiGe BiCMOS for D-Band transmitters. In Proceedings of the 2016 IEEE 16th Topical Meeting on Silicon Monolithic Integrated Circuits in RF Systems (SiRF), 24-27 January 2016, Austin, TX, USA; pp. 64–66. https://doi.org/10.1109/SIRF.2016.7445469.
112. Toupé, R.; Deval, Y.; Bégueret, J. A 125GHz LC-VCO in a SiGe:C Technology dedicated to mmW applications. In Proceedings of the 2010 IEEE Bipolar/BiCMOS Circuits and Technology Meeting (BCTM), 04-06 October 2010, Austin, TX, USA; pp. 1–4. https://doi.org/10.1109/BIPOL.2010.5668065.
113. Luo, J.; He, J.; Wang, H.; Chang, S.; Huang, Q.; Xiong, Y.-Z. A 150-GHz push-push VCO in 0.13-μm SiGe BiCMOS. In Proceedings of the 2014 International Symposium on Integrated Circuits (ISIC), 10-12 December 2014, Singapore; pp. 308–311. https://doi.org/10.1109/ISICIR.2014.7029578.
114. Kakani, V.; Jin, Y.; Dai, F.F. A 25 GHz wide-tuning VCO RFIC implemented in 0.13 um SiGe BiCMOS technology. In Proceedings of the 2010 IEEE Bipolar/BiCMOS Circuits and Technology Meeting (BCTM), 4-6 October 2010, Austin, TX, USA; pp. 5–8. https://doi.org/10.1109/BIPOL.2010.5668026.
115. Peng, Z.; Hou, D.; Chen, J.; Xiang, Y.; Hong, W. A 28 GHz Low Phase-Noise Colpitts VCO with Wide Tuning-Range in SiGe Technology. In Proceedings of the 2018 IEEE International Symposium on Radio-Frequency Integration Technology (RFIT), 15-17 August 2018, Melbourne, VIC, Australia; pp. 1–3. https://doi.org/10.1109/RFIT.2018.8524053.
116. Dyskin, A.; Wagner, S.; Kallfass, I. A Compact Resistive Quadrature Low Noise Ka-Band VCO SiGe HBT MMIC. In Proceedings of the 2019 12th German Microwave Conference (GeMiC), 25-27 March 2019, Stuttgart, Germany; pp. 95–98. https://doi.org/10.23919/GEMIC.2019.8698169.
117. Sieberhagen, D.; Nel, H.; Stander, T. A Cross-Coupled E-Band VCO with on-chip SIW Resonator in 130nm SiGe BiCMOS. In Proceedings of the 2018 IEEE Radio and Antenna Days of the Indian Ocean (RADIO), 15-18 October 2018, Wolmar, Mauritius; pp. 1–2. https://doi.org/10.23919/RADIO.2018.8572477.
118. Issakov, V.; Padovan, F. A Dual-Core 60 GHz Push-Push VCO with Second Harmonic Extraction by Mode Separation. In Proceedings of the 2018 IEEE Radio Frequency Integrated Circuits Symposium (RFIC), 10-12 June 2018, Philadelphia, PA, USA; pp. 208–211. https://doi.org/10.1109/RFIC.2018.8428832.
119. Sun, Y.; Scheytt, C.J. A low-phase-noise 61 GHz push-push VCO with divider chain and buffer in SiGe BiCMOS for 122 GHz ISM applications. In Proceedings of the 2012 IEEE Radio Frequency Integrated Circuits Symposium, 17-19 June 2012, Montreal, QC, Canada; pp. 79–82. https://doi.org/10.1109/RFIC.2012.6242236.
120. Breun, S.; Voelkel, M.; Schrotz, A.-M.; Dietz, M.; Issakov, V.; Weigel, R. A Low-Power 14% FTR Push-Push D-Band VCO in 130 nm SiGe BiCMOS Technology with -178 dBc/Hz FOMT. In Proceedings of the 2020 IEEE 20th Topical Meeting on Silicon Monolithic Integrated Circuits in RF Systems (SiRF), 26-29 January 2020, San Antonio, TX, USA; pp. 39–42. https://doi.org/10.1109/SIRF46766.2020.9040174.
121. Jamal, F.I.; Wessel, J.; Kissinger, D. A low-power K-band Colpitts VCO with 30% tuning range in a 130 nm SiGe BiCMOS technology. In Proceedings of the 2018 IEEE 18th Topical Meeting on Silicon Monolithic Integrated Circuits in RF Systems (SiRF), 14-17 January 2018, Anaheim, CA, USA; pp. 37–40. https://doi.org/10.1109/SIRF.2018.8304223.
122. Kucharski, M.; Widlok, M.; Piesiewicz, R. A W-band SiGe BiCMOS Transmitter Based on K-band Wideband VCO for Radar Applications. In Proceedings of the 2020 27th International Conference on Mixed Design of Integrated Circuits and System (MIXDES), 25-27 June 2020, Lodz, Poland; pp. 74–77. https://doi.org/10.23919/MIXDES49814.2020.9155992.
123. Ali, U.; Fischer, G.; Thiede, A. Low power fundamental VCO design in D-band using 0.13 μm SiGe BiCMOS technology. In Proceedings of the 2015 German Microwave Conference, 16-18 March 2015, Nuremberg, Germany; pp. 359–362. https://doi.org/10.1109/GEMIC.2015.7107827.
124. Sarkas, I.; Hasch, J.; Balteanu, A.; Voinigescu, S.P. A Fundamental Frequency 120-GHz SiGe BiCMOS Distance Sensor With Integrated Antenna. *IEEE Microw. Wirel. Components Lett.* **2012**, *60*, 795–812. https://doi.org/10.1109/TMTT.2011.2176504.
125. Shahramian, S.; Hart, A.; Tomkins, A.; Carusone, A. C.; Garcia, P.; Chevalier, P.; Voinigescu, S. P. Design of a Dual W- and D-Band PLL. *IEEE J. Solid-State Circuits* **2011**, *46*, 1011–1022. https://doi.org/10.1109/JSSC.2011.2117050.
126. Kucharski, M.; Eissa, M.H.; Malignaggi, A.; Wang, D.; Ng, H.J.; Kissinger, D. D-Band Frequency Quadruplers in BiCMOS Technology. *IEEE J. Solid-State Circuits* **2018**, *53*, 2465–2478. https://doi.org/10.1109/JSSC.2018.2843332.

127. Ali, U.; Bober, M.; Thiede, A. Design of voltage controlled oscillators (VCOs) in D-band and their phase noise measurements using frequency down-conversion. In Proceedings of the 2016 11th European Microwave Integrated Circuits Conference (EuMIC), 03-04 October 2016, London, UK; pp. 317–320. https://doi.org/10.1109/EuMIC.2016.7777554.
128. Ahmed, F.; Furqan, M.; Heinemann, B.; Stelzer, A. A SiGe-Based D-Band Fundamental-Wave VCO with 9 dBm Output Power and -185 dBc/Hz FoMT. In Proceedings of the 2015 IEEE Compound Semiconductor Integrated Circuit Symposium (CSICS), 11-14 October 2015, New Orleans, LA, USA; pp. 1–4. https://doi.org/10.1109/CSICS.2015.7314482.
129. Zeinolabedinzadeh, S.; Song, P.; Kaynak, M.; Kamarei, M.; Tillack, B.; Cressler, J.D. Low phase noise and high output power 367 GHz and 154 GHz signal sources in 130 nm SiGe HBT technology. In Proceedings of the 2014 IEEE MTT-S International Microwave Symposium (IMS2014), 1-6 June 2014, Tampa, FL, USA; pp. 1–4. https://doi.org/10.1109/MWSYM.2014.6848559.
130. Girma, M.G.; Hasch, J.; Gonser, M.; Sun, Y.; Zwick, T. 122 GHz single-chip dual-channel SMD radar sensor with integrated antennas for distance and angle measurements. In Proceedings of the 2014 11th European Radar Conference, 8-10 October 2014, Rome, Italy; pp. 451–454. https://doi.org/10.1109/EuRAD.2014.6991304.
131. Issakov, V.; Bilato, A.; Kurz, V.; Englisch, D.; Geiselbrechtinger, A. A Highly Integrated D-Band Multi-Channel Transceiver Chip for Radar Applications. In Proceedings of the 2019 IEEE BiCMOS and Compound semiconductor Integrated Circuits and Technology Symposium (BCICTS), 3-6 November 2019, Nashville, TN, USA; pp. 1–4. https://doi.org/10.1109/BCICTS45179.2019.8972781.
132. Hansen, S.; Bredendiek, C.; Briese, G.; Pohl, N. A Compact Harmonic Radar System With Active Tags at 61/122 GHz ISM Band in SiGe BiCMOS for Precise Localization. *IEEE Microw. Wirel. Components Lett.* **2021**, *69*, 906–915. https://doi.org/10.1109/TMTT.2020.3026353.
133. Wu, K.; Hella, M. A 103-GHz Voltage Controlled Oscillator with 28% Tuning Range and 4.2 dBm Peak Output Power Using SiGe BiCMOS Technology. In Proceedings of the 2018 IEEE/MTT-S International Microwave Symposium - IMS, 10-15 June 2018, Philadelphia, PA, USA; pp. 606–609. https://doi.org/10.1109/MWSYM.2018.8439176.
134. Schmalz, K.; Winkler, W.; Borngraber, J.; Debski, W.; Heinemann, B.; Scheytt, C. A 122 GHz receiver in SiGe technology. In Proceedings of the 2009 IEEE Bipolar/BiCMOS Circuits and Technology Meeting, 12-14 October 2009, Capri, Italy; pp. 182–185. https://doi.org/10.1109/BIPOL.2009.5314246.
135. Nasr, I.; Laemmle, B.; Knapp, H.; Fischer, G.; Weigel, R.; Kissinger, D. A wide tuning range high output power 56–74 GHz VCO with on-chip transformer load in SiGe technology. In Proceedings of the 2012 IEEE 12th Topical Meeting on Silicon Monolithic Integrated Circuits in RF Systems, 16-18 January 2012, Santa Clara, CA, USA; pp. 49–52. https://doi.org/10.1109/SiRF.2012.6160130.
136. Mahalingam, N.; Ma, K.; Yeo, K.S.; Lim, W.M. *K*-band High-PAE Wide-Tuning-Range VCO Using Triple-Coupled *LC* Tanks. *IEEE Trans. Circuits Syst. II Express Briefs* **2013**, *11*, 736–740. https://doi.org/10.1109/TCSII.2013.2281751.
137. Shin, W.; Ku, B.; Inac, O.; Ou, Y.; Rebeiz, G.M. A 108–114 GHz 4 $\times$ 4 Wafer-Scale Phased Array Transmitter With High-Efficiency On-Chip Antennas. *IEEE J. Solid-State Circuits* **2013**, *48*, 2041–2055. https://doi.org/10.1109/JSSC.2013.2260097.
138. Barghouthi, A.; Krause, A.; Carta, C.; Scheytt, C.; Ellinger, F. Design and Characterization of a V-Band Quadrature VCO Based on a Common-Collector SiGe Colpitts VCO. In Proceedings of the 2010 IEEE Compound Semiconductor Integrated Circuit Symposium (CSICS), 3-6 October 2010, Monterey, CA, USA; pp. 1–3. https://doi.org/10.1109/CSICS.2010.5619653.
139. Huang, G.; Fusco, V. A 94 GHz Wide Tuning Range SiGe Bipolar VCO Using a Self-Mixing Technique. *IEEE Microw. Wirel. Components Lett.* **2011**, *21*, 86–88. https://doi.org/10.1109/LMWC.2010.2098022.
140. Chakraborty, A.; Trotta, S.; Weigel, R. A low-phase-noise monolithically integrated 60 GHz push-push VCO for 122 GHz applications in a SiGe bipolar technology. In Proceedings of the 2013 IEEE Bipolar/BiCMOS Circuits and Technology Meeting (BCTM), 30 September 2013 - 03 October 2013, Bordeaux, France; pp. 195–198. https://doi.org/10.1109/BCTM.2013.6798174.
141. Chakraborty, A.; Trotta, S.; Wuertele, J.; Weigel, R. A D-band transceiver front-end for broadband applications in a 0.35μm SiGe bipolar technology. In Proceedings of the 2014 IEEE Radio Frequency Integrated Circuits Symposium, 1-3 June 2014, Tampa, FL, USA; pp. 405–408. https://doi.org/10.1109/RFIC.2014.6851753.
142. Bredendiek, C.; Pohl, N.; Aufinger, K.; Bilgic, A. An ultra-wideband D-Band signal source chip using a fundamental VCO with frequency doubler in a SiGe bipolar technology. In Proceedings of the 2012 IEEE Radio Frequency Integrated Circuits Symposium, 17-19 June 2012, Montreal, QC, Canada; pp. 83–86. https://doi.org/10.1109/RFIC.2012.6242237.
143. Pohl, N.; Rein, H.; Musch, T.; Aufinger, K.; Hausner, J. SiGe Bipolar VCO With Ultra-Wide Tuning Range at 80 GHz Center Frequency. *IEEE J. Solid-State Circuits* **2009**, *44*, 2655–2662. https://doi.org/10.1109/JSSC.2009.2026822.
144. Tang, X.; Nguyen, J.; Mangraviti, G.; Zong, Z.; Wambacq, P. Design and Analysis of a 140-GHz T/R Front-End Module in 22-nm FD-SOI CMOS. *IEEE J. Solid-State Circuits* **2022**, *57*, 1300–1313. https://doi.org/10.1109/JSSC.2021.3139359.
145. Tang, X.; Nguyen, J.; Medra, A.; Khalaf, K.; Visweswaran, A.; Debaillie, B.; Wambacq, P. Design of D-Band Transformer-Based Gain-Boosting Class-AB Power Amplifiers in Silicon Technologies. *IEEE Trans. Circuits Syst. I Regul. Pap.* **2020**, *67*, 1447–1458. https://doi.org/10.1109/TCSI.2020.2974197.
146. Park, S.; Park, D.-W.; Vaesen, K.; Kankuppe, A.; Sinha, S.; van Liempd, B.; Wambacq, P.; Craninckx, J. A D-Band Low-Power and High-Efficiency Frequency Multiply-by-9 FMCW Radar Transmitter in 28-nm CMOS. *IEEE Journal of Solid-State Circuits*. **2022**,*57*, 2114-2129. https://doi.org/10.1109/JSSC.2022.3157643.
147. Park, S.; Park, D. W.; Vaesen, K.; Kankuppe, A.; van Liempd, B.; Wambacq, P.; Craninckx, J. A 135–155 GHz 9.7%/16.6% DC-RF/DC-EIRP Efficiency Frequency Multiply-by-9 FMCW Transmitter in 28 nm CMOS. In Proceedings of the 2021 IEEE Radio Frequency Integrated Circuits Symposium (RFIC), 7-9 June 2021, Atlanta, GA, USA; pp. 15–18. https://doi.org/10.1109/RFIC51843.2021.9490510.

148. Dafna, Y.; Cohen, E.; Socher, E. A wideband 95–140 GHz high efficiency PA in 28nm CMOS. In Proceedings of the 2014 IEEE 28th Convention of Electrical & Electronics Engineers in Israel (IEEEI), 3-5 December 2014, Eilat, Israel; pp. 1–4. https://doi.org/10.1109/EEEI.2014.7005799.
149. Katayama, K.; Motoyoshi, M.; Takano, K.; Yang, L.C.; Fujishima, M. 133GHz CMOS power amplifier with 16dB gain and +8dBm saturated output power for multi-gigabit communication. In Proceedings of the 2013 European Microwave Integrated Circuit Conference, 6-8 October 2013, Nuremberg, Germany; pp. 69–72.
150. Simic, D.; Reynaert, P. A 14.8 dBm 20.3 dB Power Amplifier for D-band Applications in 40 nm CMOS. In Proceedings of the 2018 IEEE Radio Frequency Integrated Circuits Symposium (RFIC), 10-12 June 2018, Philadelphia, PA, USA; pp. 232–235. https://doi.org/10.1109/RFIC.2018.8428981.
151. Lee, C. J.; Kim, S. H.; Son, H. S.; Kang, D. M.; Kim, J. H.; Byeon, C. W.; Park, C. S. A 120 GHz I/Q Transmitter Front-end in a 40 nm CMOS for Wireless Chip to Chip Communication. In Proceedings of the 2018 IEEE Radio Frequency Integrated Circuits Symposium (RFIC), 10-12 June 2018, Philadelphia, PA, USA; pp. 192–195. https://doi.org/10.1109/RFIC.2018.8429019.
152. Kim, S.H.; Jang, T.H.; Kang, D.M.; Lee, C.J.; Son, H.S.; Park, C.S. A 120 GHz Wireless Radio Link for High-speed Chip-to-Chip Communication. In Proceedings of the 2019 IEEE Asia-Pacific Microwave Conference (APMC), 10-13 December 2019, Singapore; pp. 375–377. https://doi.org/10.1109/APMC46564.2019.9038678.
153. Hamani, A.; Siligaris, A.; Blampey, B.; Jimenez, J.L.G. 167-GHz and 155-GHz High Gain D-band Power Amplifiers in CMOS SOI 45-nm Technology. In Proceedings of the 2020 15th European Microwave Integrated Circuits Conference (EuMIC), 10-15 January 2021, Utrecht, Netherlands; pp. 261–264.
154. Li, S.; Rebeiz, G.M. A 130–151 GHz 8-Way Power Amplifier with 16.8–17.5 dBm Psat and 11.7–13.4% PAE Using CMOS 45nm RFSOI. In Proceedings of the 2021 IEEE Radio Frequency Integrated Circuits Symposium (RFIC), 7-9 June 2021, Atlanta, GA, USA; pp. 115–118. https://doi.org/10.1109/RFIC51843.2021.9490507.
155. Hamani, A.; Siligaris, A.; Barrera, F.; Dehos, C.; Cassiau, N.; Blampey, B.; Chaix F.; Gary, M.; Jimenez, J. L. G. A 84.48-Gb/s 64-QAM CMOS D-Band Channel-Bonding Tx Front-End With Integrated Multi-LO Frequency Generation. *IEEE Solid-State Circuits Lett.* **2020**, *3*, 346–349. https://doi.org/10.1109/LSSC.2020.3019579.
156. Shopov, S.; Gurbuz, O.D.; Rebeiz, G.M.; Voinigescu, S.P. A D -Band Digital Transmitter with 64-QAM and OFDM Free-Space Constellation Formation. *IEEE J. Solid-State Circuits* **2018**, *53*, 2012–2022. https://doi.org/10.1109/JSSC.2018.2824318.
157. Deferm, N.; Reynaert, P. A 120 GHz Fully Integrated 10 Gb/s Short-Range Star-QAM Wireless Transmitter With On-Chip Bondwire Antenna in 45 nm Low Power CMOS. *IEEE J. -Solid-State Circuits* **2014**, *49*, 1606–1616. https://doi.org/10.1109/JSSC.2014.2319250.
158. Seo, M.; Jagannathan, B.; Carta, C.; Pekarik, J.; Chen, L.; Yue, C. P.; Rodwell, M. A 1.1V 150GHz amplifier with 8dB gain and +6dBm saturated output power in standard digital 65nm CMOS using dummy-prefilled microstrip lines. In Proceedings of the 2009 IEEE International Solid-State Circuits Conference - Digest of Technical Papers, 08-12 February 2009, San Francisco, CA, USA; pp. 484–485. https://doi.org/10.1109/ISSCC.2009.4977519.
159. Luo, J.; He, J.; Feng, G.; Apriyana, A.; Fang, Y.; Xue, Z.; Huang, Q.; Yu, H. A D-Band Amplifier in 65 nm Bulk CMOS for Short-Distance Data Center Communication. *IEEE Access* **2018**, *6*, 53191–53200. https://doi.org/10.1109/ACCESS.2018.2871047.
160. Son, H. S.; Lee, C. J.; Kang, D. M.; Jang, T. H.; Lee, H.; Kim, S. H.; Byeon, C. W.; Park, C. S. A D-band CMOS power amplifier for wireless chip-to-chip communications with 22.3 dB gain and 12.2 dBm P1dB in 65-nm CMOS technology. In Proceedings of the 2018 IEEE Topical Conference on RF/Microwave Power Amplifiers for Radio and Wireless Applications (PAWR), 14-17 January 2018, Anaheim, CA, USA; pp. 35–38. https://doi.org/10.1109/PAWR.2018.8310061.
161. Meng, X.; Chi, B.; Liu, Y.; Ma, T.; Wang, Z. A Fully Integrated 150-GHz Transceiver Front-End in 65-nm CMOS. *IEEE Trans. Circuits Syst. II Express Briefs* **2019**, *66*, 602–606. https://doi.org/10.1109/TCSII.2018.2870926.
162. Yamazaki, D.; Horikawa, T.; Iizuka, T. A 140-GHz 14-dBm Power Amplifier using Power Combiner based on Symmetric Balun in 65-nm Bulk CMOS. In Proceedings of the 2020 IEEE International Symposium on Radio-Frequency Integration Technology (RFIT), 2-4 September 2020, Hiroshima, Japan; pp. 79–81. https://doi.org/10.1109/RFIT49453.2020.9226186.
163. Son, H.S.; Jang, J.Y.; Kang, D.M.; Lee, H.J.; Park, C.S. A 109 GHz CMOS Power Amplifier With 15.2 dBm Psat and 20.3 dB Gain in 65-nm CMOS Technology. *IEEE Microw. Wirel. Components Lett.* **2016**, *26*, 510–512. https://doi.org/10.1109/LMWC.2016.2574834.
164. Jiang, M.; Wen, J.; Liu, Y.; Wu, W.; Yang, D.; Sun, L. A Fully differential D-band CMOS Amplifier in 65nm bulk CMOS. In Proceedings of the 2018 11th UK-Europe-China Workshop on Millimeter Waves and Terahertz Technologies (UCMMT), 5-7 September 2018, HangZhou, China; pp. 1–3. https://doi.org/10.1109/UCMMT45316.2018.9015666.
165. Hsiao, Y.; Tsai, Z.; Liao, H.; Kao, J.; Wang, H. Millimeter-Wave CMOS Power Amplifiers With High Output Power and Wideband Performances. *IEEE Microw. Wirel. Components Lett.* **2013**, *61*, 4520–4533. https://doi.org/10.1109/TMTT.2013.2288223.
166. Philippe, B.; Reynaert, P. 24.7 A 15dBm 12.8%-PAE Compact D-Band Power Amplifier with Two-Way Power Combining in 16nm FinFET CMOS. In Proceedings of the 2020 IEEE International Solid- State Circuits Conference - (ISSCC), 16-20 February 2020, San Francisco, CA, USA; pp. 374–376. https://doi.org/10.1109/ISSCC19947.2020.9062920.
167. Ć wikliń ski, M.; Brückner, P.; Leone, S.; Friesicke, C.; Maßler, H.; Lozar, R.; Wagner, S.; Quay, R.; Ambacher, O. D-Band and G-Band High-Performance GaN Power Amplifier MMICs. *IEEE Microw. Wirel. Components Lett.* **2019**, *67*, 5080–5089. https://doi.org/10.1109/TMTT.2019.2936558.
168. Griffith, Z.; Urteaga, M.; Rowell, P. A 115–185 GHz 75–115 mW High-Gain PA MMIC in 250-nm InP HBT. In Proceedings of the 2019 49th European Microwave Conference (EuMC), 01-03 October 2019, Paris, France; pp. 860–863. https://doi.org/10.23919/EuMC.2019.8910874.

169. Ning, K.; Fang, Y.; Rodwell, M.; Buckwalter, J. A 130-GHz Power Amplifier in a 250-nm InP Process with 32% PAE. In Proceedings of the 2020 IEEE Radio Frequency Integrated Circuits Symposium (RFIC), 4-6 August 2020, Los Angeles, CA, USA; pp. 1–4. https://doi.org/10.1109/RFIC49505.2020.9218351.
170. Griffith, Z.; Urteaga, M.; Rowell, P. A 140-GHz 0.25-W PA and a 55–135 GHz 115–135 mW PA, High-Gain, Broadband Power Amplifier MMICs in 250-nm InP HBT. In Proceedings of the 2019 IEEE MTT-S International Microwave Symposium (IMS), 02-07 June 2019, Boston, MA, USA; pp. 1245–1248. https://doi.org/10.1109/MWSYM.2019.8701019.
171. Ahmed, A.S.H.; Seo, M.; Farid, A.A.; Urteaga, M.; Buckwalter, J.F.; Rodwell, M.J.W. A 140GHz power amplifier with 20.5dBm output power and 20.8% PAE in 250-nm InP HBT technology. In Proceedings of the 2020 IEEE/MTT-S International Microwave Symposium (IMS), 4-6 August 2020, Los Angeles, CA, USA; pp. 492–495. https://doi.org/10.1109/IMS30576.2020.9224012.
172. Ahmed, A.S.H.; Seo, M.; Farid, A.A.; Urteaga, M.; Buckwalter, J.F.; Rodwell, M.J.W. A 200mW D-band Power Amplifier with 17.8% PAE in 250-nm InP HBT Technology. In Proceedings of the 2020 15th European Microwave Integrated Circuits Conference (EuMIC), 10-15 January 2021, Utrecht, Netherlands; pp. 1–4. https://doi.org/10.1109/EuMIC48047.2021.00012.
173. Griffith, Z.; Urteaga, M.; Rowell, P. A Compact 140-GHz, 150-mW High-Gain Power Amplifier MMIC in 250-nm InP HBT. *IEEE Microw. Wirel. Components Lett.* **2019**, *29*, 282–284. https://doi.org/10.1109/LMWC.2019.2902333.
174. Yoon, S.; Lee, I.; Urteaga, M.; Kim, M.; Jeon, S. A Fully-Integrated 40–222 GHz InP HBT Distributed Amplifier. *IEEE Microw. Wirel. Components Lett.* **2014**, *24*, 460–462. https://doi.org/10.1109/LMWC.2014.2316223.
175. Griffith, Z.; Urteaga, M.; Rowell, P.; Tran, L. A 150–175-GHz 30-dB S_{21} Power Amplifier With 125-mW Pout and 16.2% PAE Using InP HBT. *IEEE Microwave and Wireless Components Letters*. 2022, 559–562. https://doi.org/10.1109/LMWC.2021.3140029.
176. Griffith, Z.; Urteaga, M.; Rowell, P.; Tran, L.; Brar, B. 50 – 250 GHz High-Gain Power Amplifier MMICs in 250-nm InP HBT. In Proceedings of the 2019 IEEE BiCMOS and Compound semiconductor Integrated Circuits and Technology Symposium (BCICTS), 3-6 November 2019, Nashville, TN, USA; pp. 1–6. https://doi.org/10.1109/BCICTS45179.2019.8972777.
177. Griffith, Z.; Urteaga, M.; Rowell, P. A 190-GHz High-Gain, 3-dBm OP1dB Low DC-Power Amplifier in 250-nm InP HBT. *IEEE Microw. Wirel. Components Lett.* **2017**, *27*, 1128–1130. https://doi.org/10.1109/LMWC.2017.2764739.
178. Shivan, T.; Hossain, M.; Doerner, R.; Schulz, S.; Johansen, T.; Boppel, S.; Heinrich, W.; Krozer, V. A 175 GHz Bandwidth High Linearity Distributed Amplifier in 500 nm InP DHBT Technology. In Proceedings of the 2019 IEEE MTT-S International Microwave Symposium (IMS), 2-7 June 2019, Boston, MA, USA; pp. 1253–1256. https://doi.org/10.1109/MWSYM.2019.8700895.
179. Sarkozy, S.; Vukovic, M.; Padilla, J. G.; Chang, J.; Tseng, G.; Tran, P.; Yocom, P.; Leong, K.M.K.H; Lee, W. Demonstration of a G-Band Transceiver for Future Space Crosslinks. *IEEE Transactions on Terahertz Science and Technology*, **2013**, *3*, 675–681. https://doi.org/10.1109/TTHZ.2013.2276118.
180. Samoska, L.; Peralta, A.; Hu, M.; Micovic, M.; Schmitz, A. A 20 mW, 150 GHz InP HEMT MMIC power amplifier module. *IEEE Microw. Wirel. Components Lett.* **2004**, *14*, 56–58. https://doi.org/10.1109/LMWC.2003.822575.
181. Yishay, R.B.; Elad, D. A 17.5-dBm D-band power amplifier and doubler chain in SiGe BiCMOS technology. In Proceedings of the 2014 9th European Microwave Integrated Circuit Conference, 6-7 October 2014, Rome, Italy; pp. 53–56. https://doi.org/10.1109/EuMIC.2014.6997789.
182. Yishay, R.B.; Elad, D. A 17.8 dBm 110–130 GHz Power Amplifier and doubler chain in SiGe BiCMOS technology. In Proceedings of the 2015 IEEE Radio Frequency Integrated Circuits Symposium (RFIC), 17-19 May 2015, Phoenix, AZ, USA; pp. 391–394. https://doi.org/10.1109/RFIC.2015.7337787.
183. Yishay, R.B.; Elad, D. A 240 GHz multiplier chain with -0.5 dBm output power in SiGe BiCMOS technology. In Proceedings of the 2014 9th European Microwave Integrated Circuit Conference, 6-7 October 2014, Rome, Italy; pp. 297–300. https://doi.org/10.1109/EuMIC.2014.6997851.
184. Natarajan, A.; Valdes-Garcia, A.; Sadhu, B.; Reynolds, S.K.; Parker, B.D. W-Band Dual-Polarization Phased-Array Transceiver Front-End in SiGe BiCMOS. *IEEE Microw. Wirel. Components Lett.* **2015**, *63*, 1989–2002. https://doi.org/10.1109/TMTT.2015.2422691.
185. Kucharski, M.; Ahmad, W.A.; Ng, H.J.; Kissinger, D. Monostatic and Bistatic G-Band BiCMOS Radar Transceivers With On-Chip Antennas and Tunable TX-to-RX Leakage Cancellation. *IEEE J. Solid-State Circuits* **2021**, *56*, 899–913. https://doi.org/10.1109/JSSC.2020.3041045.
186. Bao, M.; He, Z.S.; Zirath, H. A 100–145 GHz area-efficient power amplifier in a 130 nm SiGe technology. In Proceedings of the 2017 12th European Microwave Integrated Circuits Conference (EuMIC), 8-10 October 2017, Nuremberg, Germany; pp. 277–280. https://doi.org/10.23919/EuMIC.2017.8230713.
187. Visweswaran, A.; Vignon, B.; Tang, X.; Brebels, S.; Debaillie, B.; Wambacq, P. A 112–142GHz Power Amplifier with Regenerative Reactive Feedback achieving 17dBm peak Psat at 13% PAE. In Proceedings of the ESSCIRC 2019 - IEEE 45th European Solid State Circuits Conference (ESSCIRC), 23-26 September 2019, Cracow, Poland; pp. 337–340. https://doi.org/10.1109/ESSCIRC.2019.8902764.
188. Sarmah, N.; Heinemann, B.; Pfeiffer, U.R. A 135–170 GHz power amplifier in an advanced sige HBT technology. In Proceedings of the 2013 IEEE Radio Frequency Integrated Circuits Symposium (RFIC), 2-4 June 2013, Seattle, WA, USA; pp. 287–290. https://doi.org/10.1109/RFIC.2013.6569584.
189. Zhang, P.; He, L.; Guo, Y.; Fan, X.; Gao, H. A 2-stage D-band Power Amplifier with 7 dBm Output Power at 0.14 THz in a 0.13μm SiGe Technology. In Proceedings of the 2020 IEEE International Symposium on Radio-Frequency Integration Technology (RFIT), 2-4 September 2020, Hiroshima, Japan; pp. 196–198. https://doi.org/10.1109/RFIT49453.2020.9226203.

190. Hou, D.; Xiong, Y.-Z.; Goh, W.-L.; Hong, W.; Madihian, M. A D-Band Cascode Amplifier With 24.3 dB Gain and 7.7 dBm Output Power in 0.13 μm SiGe BiCMOS Technology. *IEEE Microw. Wirel. Components Lett.* **2012**, *22*, 191–193. https://doi.org/10.1109/LMWC.2012.2188624.
191. Kucharski, M.; Ng, H.J.; Kissinger, D. An 18 dBm 155–180 GHz SiGe Power Amplifier Using a 4-Way T-Junction Combining Network. In Proceedings of the ESSCIRC 2019 - IEEE 45th European Solid State Circuits Conference (ESSCIRC), 23-26 September 2019, Cracow, Poland; pp. 333–336. https://doi.org/10.1109/ESSCIRC.2019.8902847.
192. Hu, Z.; Sarris, G.; de Martino, C.; Spirito, M.; McCune, E. Design and linearity analysis of a D-band power amplifier in 0.13 μm SiGe BiCMOS technology. In Proceedings of the 2017 IEEE Compound Semiconductor Integrated Circuit Symposium (CSICS), 22-25 October 2017, Miami, FL, USA; pp. 1–4. https://doi.org/10.1109/CSICS.2017.8240469.
193. Romstadt, J.; Lammert, V.; Pohl, N.; Issakov, V. Transformer-Coupled D-Band PA with 11.8 dBm P_{sat} and 6.3 % PAE in 0.13μm SiGe BiCMOS. In Proceedings of the 2020 IEEE 20th Topical Meeting on Silicon Monolithic Integrated Circuits in RF Systems (SiRF), 26-29 January 2020, San Antonio, TX, USA; pp. 77–80. https://doi.org/10.1109/SIRF46766.2020.9040185.
194. Ali, A.; Ahmad, W.A.; Ng, H.J.; Kissinger, D.; Giannini, F.; Colantonio, P. Wideband 4-Way Combined Power Amplifier in BiCMOS Technology for D-Band Applications. In Proceedings of the 2020 IEEE Asia-Pacific Microwave Conference (APMC), 8-11 December 2020, Hong Kong; pp. 107–109. https://doi.org/10.1109/APMC47863.2020.9331364.
195. Aksoyak, I.K.; Möck, M.; Kaynak, M.; Ulusoy, A.Ç. A D-Band Power Amplifier with 15 dBm Psat in 0.13 μm SiGe BiCMOS Technology. In Proceedings of the 2022 IEEE 22nd Topical Meeting on Silicon Monolithic Integrated Circuits in RF Systems (SiRF), 16-19 January 2022, Las Vegas, NV, USA; pp. 5–8. https://doi.org/10.1109/SiRF53094.2022.9720048.
196. Karakuzulu, A.; Eissa, M.H.; Kissinger, D.; Malignaggi, A. A Broadband 110–170-GHz Stagger-Tuned Power Amplifier With 13.5-dBm Psat in 130-nm SiGe. *IEEE Microw. Wirel. Components Lett.* **2021**, *31*, 56–59. https://doi.org/10.1109/LMWC.2020.3036937.
197. Li, X.; Chen, W.; Li, S.; Wu, H.; Yi, X.; Han, R.; Feng, Z. A 110-to-130GHz SiGe BiCMOS Doherty Power Amplifier With Slotline-Based Power-Combining Technique Achieving >22dBm Saturated Output Power and >10% Power Back-off Efficiency. In Proceedings of the 2022 IEEE International Solid- State Circuits Conference (ISSCC), 20-26 February 2022, San Francisco, CA, USA; pp. 316–318. https://doi.org/10.1109/ISSCC42614.2022.9731552.
198. Furqan, M.; Ahmed, F.; Aufinger, K.; Stelzer, A. A D-band fully-differential quadrature FMCW radar transceiver with 11 dBm output power and a 3-dB 30-GHz bandwidth in SiGe BiCMOS. In Proceedings of the 2017 IEEE MTT-S International Microwave Symposium (IMS), 4-9 June 2017, Honolulu, HI, USA; pp. 1404–1407. https://doi.org/10.1109/MWSYM.2017.8058879.
199. Elkhouly, M.; Holyoak, M. J.; Hendry, D.; Zierdt, M.; Singh, A.; Sayginer, M.; Shahramian, S.; Baeyens, Y. D-band Phased-Array TX and RX Front Ends Utilizing Radio-on-Glass Technology. In Proceedings of the 2020 IEEE Radio Frequency Integrated Circuits Symposium (RFIC), 4-6 August 2020, Los Angeles, CA, USA; pp. 91–94. https://doi.org/10.1109/RFIC49505.2020.9218409.
200. Öztürk, E.; Ng, H.J.; Winkler, W.; Kissinger, D. 0.1mm2 SiGe BiCMOS RX / TX channel front-ends for 120 GHz phased array radar systems. In Proceeding of the 2017 IEEE 17th Topical Meeting on Silicon Monolithic Integrated Circuits in RF Systems (SiRF), 15-18 January 2017, Phoenix, AZ: USA; pp. 50–53. https://doi.org/10.1109/SIRF.2017.7874368.
201. Zhang, L.; Wen, J.; Sun, L.; Wu, T. A three stage, fully differential D-band power amplifier. In Proceedings of the 2014 12th IEEE International Conference on Solid-State and Integrated Circuit Technology (ICSICT), 28-31 October 2014, Guilin, China; pp. 1–3. https://doi.org/10.1109/ICSICT.2014.7021512.
202. Zhou, P.; Chen, J.; Yan, P.; Yu, J.; Li, H.; Hou, D.; Gao, H.; Hong, W. A 150-GHz Transmitter With 12-dBm Peak Output Power Using 130-nm SiGe:C BiCMOS Process. *IEEE Microw. Wirel. Components Lett.* **2020**, *68*, 3056–3067. https://doi.org/10.1109/TMTT.2020.2989112.
203. Han, J.-A.; Cheng, X.; Luo, X.-H.; Zhang, L.; Chen, F.-J.; Xia, X.-L.; Zhao, Z.C.; Chen, K.F.; Cheng, B.-B.; Deng, X.-J. A Sandwiched-Slab-Transformer-Based SiGe Power Amplifier Operating at W- and D-Bands. *IEEE Microw. Wirel. Components Lett.* **2020**, *30*, 597–600. https://doi.org/10.1109/LMWC.2020.2986920.
204. Feng, K.; Li, Q.; Xu, L. A 140GHz Power Amplifier in 0.13μm SiGe HBT technology. In Proceeding of the 2020 IEEE MTT-S International Wireless Symposium (IWS), 20-23 September 2020, Shanghai, China; pp. 1–3. https://doi.org/10.1109/IWS49314.2020.9359935.
205. Hou, D.; Hong, W.; Goh, W. L.; Xiong, Y. Z.; Annamalai Arasu, M.; He, J.; Chen, J.; Madihian, M. Distributed Modeling of Six-Port Transformer for Millimeter-Wave SiGe BiCMOS Circuits Design. *IEEE Microw. Wirel. Components Lett.* **2012**, *60*, 3728–3738. https://doi.org/10.1109/TMTT.2012.2220563.
206. Ali, A.; Yun, J.; Kucharski, M.; Ng, H.J.; Kissinger, D.; Colantonio, P. 220–360-GHz Broadband Frequency Multiplier Chains (x8) in 130-nm BiCMOS Technology. *IEEE Microw. Wirel. Components Lett.* **2020**, *68*, 2701–2715. https://doi.org/10.1109/TMTT.2020.2988869.
207. Sarmah, N.; Chevalier, P.; Pfeiffer, U. 160-GHz Power Amplifier Design in Advanced SiGe HBT Technologies With P_{sat} in Excess of 10 dBm. *IEEE Transactions on Microwave Theory and Techniques*. **2013**, *61*, 939–947. https://doi.org/10.1109/TMTT.2012.2231875.
208. Petricli, I.; Riccardi, D.; Mazzanti, A. D-Band SiGe BiCMOS Power Amplifier With 16.8dBm P1dB and 17.1% PAE Enhanced by Current-Clamping in Multiple Common-Base Stages. *IEEE Microw. Wirel. Components Lett.* **2021**, *31*, 288–291. https://doi.org/10.1109/LMWC.2021.3049458.
209. Lin, H.; Rebeiz, G.M. A 112–134 GHz SiGe amplifier with peak output power of 120 mW. In Proceeding of the 2014 IEEE Radio Frequency Integrated Circuits Symposium, 1-3 June 2014, Tampa, FL, USA; pp. 163–166. https://doi.org/10.1109/RFIC.2014.6851686.

210. Daneshgar, S.; Buckwalter, J.F. A 22 dBm, 0.6 mm^2; D-Band SiGe HBT Power Amplifier Using Series Power Combining Sub-Quarter-Wavelength Baluns. In Proceeding of the 2015 IEEE Compound Semiconductor Integrated Circuit Symposium (CSICS), 11-14 October 2015, New Orleans, LA, USA; pp. 1–4. https://doi.org/10.1109/CSICS.2015.7314467.
211. Rao, S.G.; Cressler, J.D. A D-Band SiGe Power Amplifier Using a Four-Way Coupled-Line Wilkinson Combiner. *IEEE Microw. Wirel. Components Lett.* **2021**, *31*, 1239–1242. https://doi.org/10.1109/LMWC.2021.3097017.
212. Ali, A.; Yun, J.; Ng, H.J.; Kissinger, D.; Giannini, F.; Colantonio, P. 90 GHz Bandwidth Single-Ended PA for D-Band Applications in BiCMOS Technology. In Proceeding of the 2020 4th Australian Microwave Symposium (AMS), 13-14 February 2020, Sydney, NSW, Australia; pp. 1–2. https://doi.org/10.1109/AMS48904.2020.9059473.
213. Yishay, R.B.; Elad, D. A 230 GHz quadrupler with 2 dBm output power in 90 nm SiGe BiCMOS technology. In Proceeding of the 2016 11th European Microwave Integrated Circuits Conference (EuMIC), 3-4 October 2016, London, UK; pp. 101–104. https://doi.org/10.1109/EuMIC.2016.7777500.
214. Lin, H.; Rebeiz, G.M. A 110–134-GHz SiGe Amplifier With Peak Output Power of 100–120 mW. *IEEE Microw. Wirel. Components Lett.* **2014**, *62*, 2990–3000. https://doi.org/10.1109/TMTT.2014.2360679.
215. Huang, D.; Zhang, L.; Zhu, H.; Chen, B.; Tang, Y.; Wang, Y. A 94GHz 2×2 Phased-Array FMCW Imaging Radar Transceiver with 11dBm Output Power and 10.5dB NF in 65nm CMOS. In Proceeding of the 2019 IEEE Radio Frequency Integrated Circuits Symposium (RFIC), 2-4 June 2019, Boston, MA, USA; pp. 47–50. https://doi.org/10.1109/RFIC.2019.8701876.
216. Su, Y.; Tsai, M.; Wu, J.; Chin, T.; Chang, C. A V-/W-band 0.18-μm CMOS phase shifter MMIC with 180°-300° phase tuning range. In Proceeding of the 2012 Asia Pacific Microwave Conference Proceedings, 4-7 December 2012, Kaohsiung, Taiwan; pp. 91–93. https://doi.org/10.1109/APMC.2012.6421508.
217. Vahdati, A.; Lamminen, A.; Varonen, M.; Säily, J.; Lahti, M.; Kautio, K.; Lahdes, M.; Parveg, D.; Karaca, D.; Halonen, K.A.I. 90 GHz CMOS Phased-Array Transmitter Integrated on LTCC. *IEEE Trans. Antennas Propag.* **2017**, *65*, 6363–6371. https://doi.org/10.1109/TAP.2017.2743009.
218. Vahdati, A.; Parveg, D.; Varonen, M.; Kärkkäinen, M.; Karaca, D.; Halonen, K.A.I. A 100-GHz phase shifter in 28-nm CMOS FDSOI. In Proceeding of the 2015 10th European Microwave Integrated Circuits Conference (EuMIC), 7-8 September 2015, Paris, France; pp. 112–115. https://doi.org/10.1109/EuMIC.2015.7345081.
219. Pepe, D.; Zito, D. A 78.8–92.8 GHz 4-bit 0–360° active phase shifter in 28nm FDSOI CMOS with 2.3 dB average peak gain. In Proceeding of the ESSCIRC Conference 2015 - 41st European Solid-State Circuits Conference (ESSCIRC), 14-18 September 2015, Graz, Austria; pp. 64–67. https://doi.org/10.1109/ESSCIRC.2015.7313829.
220. Vahdati, A.; Varonen, M.; Kärkkäinen, M.; Parveg, D.; Halonen, K.A.I. A 97–106-GHz differential I-Q phase shifter in 28-nm CMOS. In Proceeding of the 2014 NORCHIP, 27-28 October 2014, Tampere, Finland; pp. 1–4. https://doi.org/10.1109/NORCHIP.2014.7004724.
221. Sung, E.; Hong, S. A Wideband W-band 6-bit Active Phase Shifter in 28-nm RF CMOS. In Proceeding of the 2019 IEEE International Symposium on Radio-Frequency Integration Technology (RFIT), 28-30 August 2019, Nanjing, China; pp. 1–3. https://doi.org/10.1109/RFIT.2019.8929156.
222. de Wit, M.; Reynaert, P. An F-band active phase shifter in 28nm CMOS. In Proceeding of the 2017 IEEE MTT-S International Microwave Symposium (IMS), 04-09 June 2017, Honololu, HI, USA; pp. 965–968. https://doi.org/10.1109/MWSYM.2017.8058750.
223. Vahdati, A.; Varonen, M.; Kärkkäinen, M.; Halonen, K.A.I. Design of a W-Band 2-bit differential CMOS phase shifter. In Proceeding of the 2013 9th Conference on Ph.D. Research in Microelectronics and Electronics (PRIME), 24-27 June 2013, Villach, Austria; pp. 97–100. https://doi.org/10.1109/PRIME.2013.6603111.
224. Sayginer, M.; Rebeiz, G.M. A 94–96 GHz phased-array receive front-end with 5-bit phase control and 5 dB noise figure in 32 nm CMOS SOI. In Proceeding of the 2017 IEEE MTT-S International Microwave Symposium (IMS), 4-9 June 2017, Honololu, HI, USA; pp. 768–770. https://doi.org/10.1109/MWSYM.2017.8058690.
225. Huang, C.-Y.; Hsieh, K.-H.; Hu, R. 40 nm-CMOS W-band Phase Shifter for Millimeter-wave Phased Array. In Proceeding of the 2019 PhotonIcs & Electromagnetics Research Symposium-Spring (PIERS-Spring), 17-20 June 2019, Rome, Italy; pp. 1700–1705. https://doi.org/10.1109/PIERS-Spring46901.2019.9017537.
226. Zhou, J.; Qian, H.J.; Luo, X. A 9-Bit Vector-Sum Digital Phase Shifter Using High Resolution VGAs and Compensated Quadrature Signal Generator. In Proceeding of the 2019 IEEE MTT-S International Microwave Conference on Hardware and Systems for 5G and Beyond (IMC-5G), 15-16 August 2019, Atlanta, GA, USA; pp. 1–3. https://doi.org/10.1109/IMC-5G47857.2019.9160356.
227. Zhu, W.; Wang, J.; Wang, R.; Wang, Y. 14.5 A 1V W-Band Bidirectional Transceiver Front-End with <1dB T/R Switch Loss, <1°/dB Phase/Gain Resolution and 12.3% TX PAE at 15.1dBm Output Power in 65nm CMOS Technology. In Proceeding of the 2021 IEEE International Solid- State Circuits Conference (ISSCC), 13-22 February 2021, San Francisco, CA, USA; pp. 226–228. https://doi.org/10.1109/ISSCC42613.2021.9365944.
228. Lee, H.; Min, B. W-Band CMOS 4-Bit Phase Shifter for High Power and Phase Compression Points. *IEEE Trans. Circuits Syst. II Express Briefs* **2015**, *62*, 1–5. https://doi.org/10.1109/TCSII.2014.2362732.
229. Shih, S.E.; Duan, D. W.; Fordham, O.; Parmar, M.; Tornquist, K.; Zeng, X.; Chang-Chien, P.; Tsai, R. A W-Band 4-Bit Phase Shifter in Multilayer Scalable Array Systems. 2007 IEEE Compound Semiconductor Integrated Circuits Symposium, 2007; pp. 1–4. https://doi.org/10.1109/CSICS07.2007.20.

230. Müller, D.; Diebold, S.; Reiss, S.; Massler, H.; Tessmann, A.; Leuther, A.; Zwick, T.; Kallfass, I. D-Band digital phase shifters for phased-array applications. In Proceeding of the 2015 German Microwave Conference, 16-18 March 2015, Nuremberg, Germany; pp. 205–208. https://doi.org/10.1109/GEMIC.2015.7107789.
231. Müller, D.; Längst, J.; Tessmann, A.; Leuther, A.; Zwick, T.; Kallfass, I. A D-Band 180° phase shifter with very low amplitude- and phase-error. In Proceeding of the 2014 9th European Microwave Integrated Circuit Conference, 06-07 October 2014, Rome, Italy; pp. 174–177. https://doi.org/10.1109/EuMIC.2014.6997820.
232. Margomenos, A.; Kurdoghlian, A.; Micovic, M.; Shinohara, K.; Moyer, H.; Regan, D. C.; Grabar, R. M.; McGuire, C.; Wetzel, M. D.; Chow, D. H. W-Band GaN Receiver Components Utilizing Highly Scaled, Next Generation GaN Device Technology. In Proceeding of the 2014 IEEE Compound Semiconductor Integrated Circuit Symposium (CSICS), 19-22 October 2014, La Jolla, CA, USA; pp. 1–4. https://doi.org/10.1109/CSICS.2014.6978585.
233. Thome, F.; Diebold, S.; Schlechtweg, M.; Leuther, A.; Ambacher, O.; Kallfass, I. A tunable 140GHz analog phase shifter with high linearity performance. In Proceeding of the 2012 The 7th German Microwave Conference, 12-14 March 2012, Ilmenau, Germany; pp. 1–4.
234. Parlak, M.; Buckwalter, J.F. A Low-Power, W-Band Phase Shifter in a 0.12 μm SiGe BiCMOS Process. *IEEE Microw. Wirel. Components Lett.* **2010**, *20*, 631–633. https://doi.org/10.1109/LMWC.2010.2066552.
235. Yishay, R.B.; Elad, D. D-Band 360° Phase Shifter with Uniform Insertion Loss. In Proceeding of the 2018 IEEE/MTT-S International Microwave Symposium - IMS, 10-15 June 2018, Philadelphia, PA, USA; pp. 868–870. https://doi.org/10.1109/MWSYM.2018.8439838.
236. Kim, S.Y.; Rebeiz, G.M. A Low-Power BiCMOS 4-Element Phased Array Receiver for 76–84 GHz Radars and Communication Systems. *IEEE J. Solid-State Circuits* **2012**, *47*, 359–367. https://doi.org/10.1109/JSSC.2011.2170769.
237. Venter, J.J.P.; Stander, T. W-band capacitively loaded slow-wave transmission line phase shifter in 130nm CMOS. In Proceeding of the 2017 IEEE AFRICON, 18-20 September 2017, Cape Town, South Africa; pp. 555–558. https://doi.org/10.1109/AFRCON.2017.8095541.
238. SeyyedEsfahlan, M.; Öztürk, E.; Kaynak, M.; Tekin, I. 77-GHz Four-Element Phased-Array Radar Receiver Front End. *IEEE Trans. Components, Packag. Manuf. Technol.* **2016**, *6*, 1162–1173. https://doi.org/10.1109/TCPMT.2016.2571742.
239. Afroz, S.; Koh, Kw. 90° hybrid-coupler based phase-interpolation phase-shifter for phased-array applications at W-band and beyond. In Proceeding of the 2016 IEEE MTT-S International Microwave Symposium (IMS), 22-27 May 2016, San Francisco, CA, USA; pp. 1–4. https://doi.org/10.1109/MWSYM.2016.7540415.
240. Testa, P.V.; Carta, C.; Ellinger, F. A 140–210 GHz Low-Power Vector-Modulator Phase Shifter in 130nm SiGe BiCMOS Technology. In Proceeding of the 2018 Asia-Pacific Microwave Conference (APMC), 6-9 November 2018, Kyoto, Japan; pp. 530–532. https://doi.org/10.23919/APMC.2018.8617631.
241. Zhang, Z.; Xie, Q.; Wang, Z. A 150–170GHz 5-Bit Vector-Modulated Phase Shifter Based on X-type Phase Inverter Technique. In Proceeding of the 2021 IEEE International Conference on Integrated Circuits, Technologies and Applications (ICTA), 24-26 November 2021, Zhuhai, China; pp. 22–23. https://doi.org/10.1109/ICTA53157.2021.9661987.
242. Testa, P.V.; Carta, C.; Ellinger, F. A 160–190-GHz Vector-Modulator Phase Shifter for Low-Power Applications. *IEEE Microw. Wirel. Components Lett.* **2020**, *30*, 86–89. https://doi.org/10.1109/LMWC.2019.2952766.
243. Golcuk, F.; Kanar, T.; Rebeiz, G.M. A 90–100 Ghz 4×4 sige BiCMOS polarimetric transmit-receive phased array with simultaneous receive-beams capabilities. In Proceeding of the 2013 IEEE International Symposium on Phased Array Systems and Technology, 15-18 October 2013, Waltham, MA, USA; pp. 102–105. https://doi.org/10.1109/ARRAY.2013.6731809.
244. Afroz, S.; Koh, K.-J. A *D* -Band Two-Element Phased-Array Receiver Front End With Quadrature-Hybrid-Based Vector Modulator. *IEEE Microw. Wirel. Components Lett.* **2018**, *28*, 180–182. https://doi.org/10.1109/LMWC.2018.2792150.
245. Li, H.; Chen, J.; Hou, D.; Hong, W. A W-Band 6-Bit Phase Shifter With 7 dB Gain and 1.35° RMS Phase Error in 130 nm SiGe BiCMOS. *IEEE Trans. Circuits Syst. II Express Briefs* **2020**, *67*, 1839–1843. https://doi.org/10.1109/TCSII.2019.2944166.
246. Karakuzulu, A.; Eissa, M.H.; Kissinger, D.; Malignaggi, A. Broadband 110 - 170 GHz True Time Delay Circuit in a 130-nm SiGe BiCMOS Technology. In Proceeding of the 2020 IEEE/MTT-S International Microwave Symposium (IMS), 4-6 August 2020, Los Angeles, CA, USA; pp. 775–778. https://doi.org/10.1109/IMS30576.2020.9223843.
247. Stärke, P.; Rieß, V.; Carta, C.; Ellinger, F. Continuous 360° Vector Modulator with Passive Phase Generation for 140 GHz to 200 GHz G-Band. In Proceeding of the 2019 12th German Microwave Conference (GeMiC), 25-27 March 2019, Stuttgart, Germany; pp. 240–243. https://doi.org/10.23919/GEMIC.2019.8698129.
248. Karakuzulu, A.; Eissa, M.H.; Kissinger, D.; Malignaggi, A. Full D-Band Transmit–Receive Module for Phased Array Systems in 130-nm SiGe BiCMOS. *IEEE Solid-State Circuits Lett.* **2021**, *4*, 40–43. https://doi.org/10.1109/LSSC.2021.3054512.
249. Afroz, S.; Kim, H.; Koh, K.-J. Power-Efficient W -Band (92–98 GHz) Phased-Array Transmit and Receive Elements With Quadrature-Hybrid-Based Passive Phase Interpolator. *IEEE J. Solid-State Circuits* **2018**, *53*, 1678–1693. https://doi.org/10.1109/JSSC.2018.2810178.
250. Maiwald, T.; Kolb, K.; Potschka, J.; Dietz, M.; Weigel, R. Towards Broadband D-Band Wireless Communication Systems using Beam Steering in SiGe BiCMOS Technology. In Proceeding of the 2021 13th Global Symposium on Millimeter-Waves & Terahertz (GSMM), 23-26 May 2021, Nanjing, China; pp. 1–3. https://doi.org/10.1109/GSMM53250.2021.9512012.
251. Deng, X.; He, Z.; Yuan, S.; Shao, Z.; Liu, L. W-band high bit passive phase shifter for automotive radar applications in BiCMOS. In Proceeding of the 2011 International Conference on Computational Problem-Solving (ICCP), 21-23 October 2011, Chengdu, China; pp. 115–119. https://doi.org/10.1109/ICCPS.2011.6092220.

252. Shahramian, S.; Baeyens, Y.; Chen, Y. A 70–100GHz direct-conversion transmitter and receiver phased array chipset in 0.18μm SiGe BiCMOS technology. In Proceeding of the 2012 IEEE Radio Frequency Integrated Circuits Symposium, 17-19 June 2012, Montreal, QC, Canada; pp. 123–126. https://doi.org/10.1109/RFIC.2012.6242246.
253. Elkhouly, M.; Glisic, S.; Ellinger, F.; Scheytt, J.C. 120 GHz phased-array circuits in 0.25 μm SiGe BiCMOS technology. In Proceeding of the 2012 The 7th German Microwave Conference, 12-14 March 2012, Ilmenau, Germany; pp. 1–4.
254. Rio, D.d.; Gurutzeaga, I.; Berenguer, R.; Huhtinen, I.; Sevillano, J.F. A Compact and High-Linearity 140–160 GHz Active Phase Shifter in 55 nm BiCMOS. *IEEE Microw. Wirel. Components Lett.* **2021**, *31*, 157–160. https://doi.org/10.1109/LMWC.2020.3037162.
255. Farid, A.A.; Simsek, A.; Ahmed, A.S.H.; Rodwell, M.J.W. A Broadband Direct Conversion Transmitter/Receiver at D-band Using CMOS 22nm FDSOI. In Proceeding of the 2019 IEEE Radio Frequency Integrated Circuits Symposium (RFIC), 2-4 June 2019, Boston, MA, USA; pp. 135–138. https://doi.org/10.1109/RFIC.2019.8701730.
256. Landsberg, N.; Asaf, O.; Shin, W. A D-Band LNA Using a 22 nm FD-SOI CMOS Technology for Radar Applications. In Proceeding of the 2021 IEEE International Conference on Microwaves, Antennas, Communications and Electronic Systems (COMCAS), 1-3 November 2021, Tel Aviv, Israel; pp. 178–180. https://doi.org/10.1109/COMCAS52219.2021.9629055.
257. Wang, C.; Rebeiz, G. A 2-Channel 136–156 GHz Dual Down-Conversion I/Q Receiver with 30 dB Gain and 9.5 dB NF Using CMOS 22nm FDSOI. In Proceeding of the 2021 IEEE Radio Frequency Integrated Circuits Symposium (RFIC), 7-9 June 2021, Atlanta, GA, USA; pp. 219–222. https://doi.org/10.1109/RFIC51843.2021.9490408.
258. Wu, L.; Hsu, H.Y.; Voinigescu, S.P. A DC to 220-GHz High-Isolation SPST Switch in 22-nm FDSOI CMOS. *IEEE Microw. Wirel. Components Lett.* **2021**, *31*, 775–778. https://doi.org/10.1109/LMWC.2021.3067003.
259. Heller, T.; Cohen, E.; Socher, E. A 102–129-GHz 39-dB Gain 8.4-dB Noise Figure I/Q Receiver Frontend in 28-nm CMOS. *IEEE Microw. Wirel. Components Lett.* **2016**, *64*, 1535–1543. https://doi.org/10.1109/TMTT.2016.2547390.
260. Kankuppe, A.; Park, S.; Vaesen, K.; Park, D.-W.; Van Liempd, B.; Wambacq, P.; Craninckx, J. A 67mW D-band FMCW I/Q Radar Receiver with an N-path Spillover Notch Filter in 28nm CMOS. In Proceeding of the ESSCIRC 2021 - IEEE 47th European Solid State Circuits Conference (ESSCIRC), 13-22 September 2021, Grenoble, France; pp. 471–474. https://doi.org/10.1109/ESSCIRC53450.2021.9567860.
261. Sayginer, M.; Rebeiz, G.M. A W-Band LNA/Phase Shifter With 5-dB NF and 24-mW Power Consumption in 32-nm CMOS SOI. *IEEE Microw. Wirel. Components Lett.* **2018**, *66*, 1973–1982. https://doi.org/10.1109/TMTT.2018.2799842.
262. Hamani, A.; Siligaris, A.; Blampey, B.; Dehos, C.; Jimenez, J.L.G. A 125.5–157 GHz 8 dB NF and 16 dB of Gain D-band Low Noise Amplifier in CMOS SOI 45 nm. In Proceeding of the 2020 IEEE/MTT-S International Microwave Symposium (IMS), 4-6 August 2020, Los Angeles, CA, USA; pp. 197–200. https://doi.org/10.1109/IMS30576.2020.9224114.
263. Hamani, A.; Siligaris, A.; Dehos, C.; Cassiau, N.; Blampey, B.; Chaix, F.; Gary, M.; Gonzalez-Jimenez, J. L. A 108-Gb/s 64-QAM CMOS D-Band Rx With Integrated LO Generation. *IEEE Solid-State Circuits Lett.* **2020**, *3*, 202–205. https://doi.org/10.1109/LSSC.2020.3011529.
264. Liu, H.; Meng, F.; Fu, H. A D-Band Wideband High-Gain Low-Noise Amplifier in 55-nm CMOS. In Proceeding of the 2020 13th UK-Europe-China Workshop on Millimetre-Waves and Terahertz Technologies (UCMMT), 29 August - 1 September 2020, Tianjin, China; pp. 1–4. https://doi.org/10.1109/UCMMT49983.2020.9296062.
265. Katayama, K.; Takano, K.; Amakawa, S.; Yoshida, T.; Fujishima, M. 14.4-dB CMOS D-band low-noise amplifier with 22.6-mW power consumption utilizing bias-optimization technique. In Proceeding of the 2016 IEEE International Symposium on Radio-Frequency Integration Technology (RFIT), 24-26 August 2016, Taipei, Taiwan; pp. 1–3. https://doi.org/10.1109/RFIT.2016.7578218.
266. Lee, C.J.; Jang, T.H.; Kang, D.M.; Son, H.S.; Byeon, C.W.; Park, C.S. A CMOS D-band low noise amplifier with 22.4dB gain and a 3dB bandwidth of 16GHz for wireless chip to chip communication. In Proceeding of the 2017 Progress in Electromagnetics Research Symposium - Fall (PIERS - FALL), 19-22 November 2017, Singapore; pp. 2339–2343. https://doi.org/10.1109/PIERS-FALL.2017.8293527
267. Elkind, J.; Socher, E. A 154–165 GHz LNA and receiver in CMOS 65 nm technology. In Proceeding of the 2016 11th European Microwave Integrated Circuits Conference (EuMIC), 03-04 October 2016, London, UK; pp. 393–396. https://doi.org/10.1109/EuMIC.2016.7777574.
268. Kim, D.; Kim, D.; Rieh, J. A *D* -Band CMOS Amplifier With a New Dual-Frequency Interstage Matching Technique. *IEEE Microw. Wirel. Components Lett.* **2017**, *65*, 1580–1588. https://doi.org/10.1109/TMTT.2017.2655508.
269. Yun, B.; Park, D.-W.; Mahmood, H.U.; Kim, D.; Lee, S.-G. A D-Band High-Gain and Low-Power LNA in 65-nm CMOS by Adopting Simultaneous Noise- and Input-Matched Gmax-Core. *IEEE Microw. Wirel. Components Lett.* **2021**, *69*, 2519–2530. https://doi.org/10.1109/TMTT.2021.3066972.
270. Orii, A.; Katayama, K.; Motoyoshi, M.; Takano, K.; Fujishima, M. 118GHz CMOS amplifier with group delay variation of 11.2ps and 3dB bandwidth of 20.4GHz. In Proceeding of the 2012 IEEE International Meeting for Future of Electron Devices, Kansai, 9-11 May 2012, Suita, Japan; pp. 1–2. https://doi.org/10.1109/IMFEDK.2012.6218630.
271. Vassilev, V.; Wadefalk, N.; Abbasi, M.; Kozhuharov, R.; Zirath, H.; Gunnarsson, S. E.; Pellikka, T.; Emrich, A.; Kallfass, I.; Leuther, A. Integrated front-ends up to 200 GHz. In Proceeding of the 2011 IEEE MTT-S International Microwave Workshop Series on Millimeter Wave Integration Technologies, 15-16 September 2011, Sitges, Spain; pp. 57–60. https://doi.org/10.1109/IMWS3.2011.6061886.
272. Cleriti, R.; Ciccognani, W.; Colangeli, S.; Serino, A.; Limiti, E.; Frijlink, P.; Renvoisé, M.; Doerner, R.; Hossain, M. D-band LNA using a 40-nm GaAs mHEMT technology. In Proceeding of the 2017 12th European Microwave Integrated Circuits Conference (EuMIC), 8-10 October 2017, Nuremberg, Germany; pp. 105–108. https://doi.org/10.23919/EuMIC.2017.8230671.

273. Weber, R.;Cwiklinski, M.; Wagner, S.; Lozar, S.; Massler, H.; Brückner, P.; Quay, R. A Beyond 110 GHz GaN Cascode Low-Noise Amplifier with 20.3 dBm Output Power. In Proceeding of the 2018 IEEE/MTT-S International Microwave Symposium-IMS, 10-15 June 2018, Philadelphia, PA, USA; pp. 1499–1502. https://doi.org/10.1109/MWSYM.2018.8439698.
274. Kurdoghlian, A.; Moyer, H.; Sharifi, H.; Brown, D. F.; Nagele, R.; Tai, J.; Bowen, R.; Wetzel, M.; Grabar, R.; Santos, D.; et al. First demonstration of broadband W-band and D-band GaN MMICs for next generation communication systems. In Proceeding of the 2017 IEEE MTT-S International Microwave Symposium (IMS), 4-9 June 2017, Honololu, HI, USA; pp. 1126–1128. https://doi.org/10.1109/MWSYM.2017.8058796.
275. Andrić, S.; Fhager, L.O.; Wernersson, L.-E. Millimeter-Wave Vertical III-V Nanowire MOSFET Device-to-Circuit Co-Design. *IEEE Trans. Nanotechnol.* **2021**, *20*, 434–440. https://doi.org/10.1109/TNANO.2021.3080621.
276. Stärke, P.; Carta, C.; Ellinger, F. 180 GHz HBT MMIC Amplifier with 80 GHz Bandwidth and Low Noise Figure in 250 nm InP. In Proceeding of the 2019 European Microwave Conference in Central Europe (EuMCE), 13-15 May 2019, Prague, Czech Republic; pp. 99–102.
277. Hassona, A.; Vassilev, V.; Zaman, A. U.; Yan, Y.; An, S.; He, Z. S.; Habibpour, O.; Carpenter, S.; Bao, M.; Zirath, H. Nongalvanic Generic Packaging Solution Demonstrated in a Fully Integrated D-Band Receiver. *IEEE Trans. Terahertz Sci. Technol.* **2020**, *10*, 321–330. https://doi.org/10.1109/TTHZ.2020.2972362.
278. Watson, P.; Mattamana, A.; Gilbert, R.; Royter, Y.; Lau, M.; Valles, I.; Li, J. A wide-bandwidth W-band LNA in InP/Si BiCMOS technology. In Proceeding of the 2014 IEEE MTT-S International Microwave Symposium (IMS2014), 1-6 June 2014, Tampa, FL, USA; pp. 1–4. https://doi.org/10.1109/MWSYM.2014.6848249.
279. Yang, D.; Wen, J.; He, M.; He, R. A D-band Monolithic Low Noise Amplifier on InP HEMT Technology. In Proceeding of the 2018 12th International Symposium on Antennas, Propagation and EM Theory (ISAPE), 3-6 December 2018, Hangzhou, China; pp. 1–4. https://doi.org/10.1109/ISAPE.2018.8634087.
280. Wang, Y.; Wu, H.; Li, J.; Fu, X. The D-band MMIC LNA circuit using 70nm InP HEMT technology. In Proceeding of the 2017 IEEE 12th International Conference on ASIC (ASICON), 25-28 October 2017, Guiyang, China; pp. 887–890. https://doi.org/10.1109/ASICON.2017.8252619.
281. Eskanadri, S.; Hamedani, F.T. Design and progress of a wideband 120–210 GHz low noise amplifier. In Proceeding of the 2012 19th International Conference on Microwaves, Radar & Wireless Communications, 21-23 May 2012, Warsaw, Poland; pp. 757–760. https://doi.org/10.1109/MIKON.2012.6233630.
282. Sato, M.; Shiba, S.; Matsumura, H.; Takahashi, T.; Suzuki, T.; Nakasha, Y.; Hara, N. Submillimeter-wave InP HEMT amplifiers with current-reuse topology. In Proceeding of the 2013 IEEE Topical Conference on Power Amplifiers for Wireless and Radio Applications, 21-23 January 2013, Austin, TX, USA; pp. 79–81. https://doi.org/10.1109/PAWR.2013.6490195.
283. Sato, M.; Takahashi, T.; Hirose, T. 68–110-GHz-Band Low-Noise Amplifier Using Current Reuse Topology. *IEEE Microw. Wirel. Components Lett.* **2010**, *58*, 1910–1916. https://doi.org/10.1109/TMTT.2010.2050374.
284. Yishay, R.B.; Elad, D. A 95–135 GHz Low Power Dicke Radiometer in SiGe BiCMOS Technology. In Proceeding of the 2020 15th European Microwave Integrated Circuits Conference (EuMIC), 10-15 January 2021, Utrecht, Netherlands; pp. 133–136.
285. Shumakher, E.; Elad, D. Towards a 120 GHz SiGe LNA for millimeter-wave imaging. In Proceeding of the 2011 IEEE International Conference on Microwaves, Communications, Antennas and Electronic Systems (COMCAS 2011), 7-9 November 2011, Tel Aviv, Israel; pp. 1–4. https://doi.org/10.1109/COMCAS.2011.6105821.
286. Aguilar, E.; Hagelauer, A.; Kissinger, D.; Weigel, R. A low-power wideband D-band LNA in a 130 nm BiCMOS technology for imaging applications. In Proceeding of the 2018 IEEE 18th Topical Meeting on Silicon Monolithic Integrated Circuits in RF Systems (SiRF), 14-17 January 2018, Anaheim, CA, USA; pp. 27–29. https://doi.org/10.1109/SIRF.2018.8304220.
287. Ustundag, B.; Turkmen, E.; Cetindogan, B.; Guner, A.; Kaynak, M.; Gurbuz, Y. Low-Noise Amplifiers for W-Band and D-Band Passive Imaging Systems in SiGe BiCMOS Technology. In Proceeding of the 2018 Asia-Pacific Microwave Conference (APMC), 6-9 November 2018, Kyoto, Japan; pp. 651–653. https://doi.org/10.23919/APMC.2018.8617582.
288. Ulusoy, A.Ç.; Song, P.; Khan, W. T.; Kaynak, M.; Tillack, B.; Papapolymerou, J.; Cressler, J. D. A SiGe D-Band Low-Noise Amplifier Utilizing Gain-Boosting Technique. *IEEE Microw. Wirel. Components Lett.* **2015**, *25*, 61–63. https://doi.org/10.1109/LMWC.2014.2369992.
289. Turkmen, E.; Burak, A.; Guner, A.; Kalyoncu, I.; Kaynak, M.; Gurbuz, Y. A SiGe HBT D -Band LNA With Butterworth Response and Noise Reduction Technique. *IEEE Microw. Wirel. Components Lett.* **2018**, *28*, 524–526. https://doi.org/10.1109/LMWC.2018.2831450.
290. Maiwald, T.; Potschka, J.; Kolb, K.; Dietz, M.; Aufinger, K.; Visweswaran, A.; Weigel, R. A Full D-Band Low Noise Amplifier in 130 nm SiGe BiCMOS using Zero-Ohm Transmission Lines. In Proceeding of the 2020 15th European Microwave Integrated Circuits Conference (EuMIC), 10-15 January 2021, Utrecht, Netherlands; pp. 13–16.
291. Ding, T.; Meng, F.; Ma, K.; Mou, S.; Xu, S. A 0.1 THz SiGe LNA with Novel Feedback Networks for Bandwidth Extension. In Proceeding of the 2019 IEEE Asia-Pacific Microwave Conference (APMC), 10-13 December 2019, Singapore; pp. 1685–1687. https://doi.org/10.1109/APMC46564.2019.9038633.
292. Liu, G.; Schumacher, H. 47–77 GHz and 70–155 GHz LNAs in SiGe BiCMOS technologies. In Proceeding of the 2012 IEEE Bipolar/BiCMOS Circuits and Technology Meeting (BCTM), 30 September - 3 October 2012, Portland, OR, USA; pp. 1–4. https://doi.org/10.1109/BCTM.2012.6352641.

293. Öjefors, E.; Pourchon, F.; Chevalier, P.; Pfeiffer, U.R. A 160-GHz low-noise downconverter in a SiGe HBT technology. In Proceeding of the 40th European Microwave Conference, 28-30 September 2010, Paris, France; pp. 521–524. https://doi.org/10.23919/EUMC.2010.5616483.
294. Liu, B.; Mou, S.; Ma, K.; Meng, F. A D-band SiGe differential amplifier with 20 dB power gain and 30 GHz bandwidth. In Proceeding of the 2017 Progress in Electromagnetics Research Symposium - Fall (PIERS - FALL), 19-22 November 2017, Singapore; pp. 548–552. https://doi.org/10.1109/PIERS-FALL.2017.8293198.
295. Aguilar, E.; Issakov, V.; Weigel, R. Highly-Integrated <0.14mm2D -Band Receiver Front-Ends for Radar and Imaging Applications in a 130 nm SiGe BiCMOS Technology. In Proceeding of the 2019 IEEE 19th Topical Meeting on Silicon Monolithic Integrated Circuits in RF Systems (SiRF), 20-23 January 2019, Orlando, FL, USA; pp. 1–4. https://doi.org/10.1109/SIRF.2019.8709129.
296. Valenta, V.; Winkler, W.; Spreng, T.; Dancila, D.; Kaynak, M.; Yuan, S.; Trasser, A.; Rydberg, A.; Schumacher, H. High performance transmit/receive modules in 0.13 μm SiGe:C BiCMOS for short range F-band MIMO radars. In Proceeding of the 2014 IEEE MTT-S International Microwave Symposium (IMS2014), 1-6 June 2014, Tampa, FL, USA; pp. 1–3. https://doi.org/10.1109/MWSYM.2014.6848432.
297. Testa, P.V.; Riess, V.; Carta, C.; Ellinger, F. A 130 nm-SiGe-BiCMOS Low-Power Receiver Based on Distributed Amplifier Techniques for Broadband Applications From 140 GHz to 200 GHz. *IEEE Open J. Circuits Syst.* **2021**, *2*, 508–519. https://doi.org/10.1109/OJCAS.2021.3103604.
298. Stärke, P.; Seidel, A.; Carta, C.; Ellinger, F. Direct-Conversion Receiver Front-End for 180 GHz with 80 GHz Bandwidth in 130nm SiGe. In Proceeding of the 2019 IEEE Asian Solid-State Circuits Conference (A-SSCC), 4-6 November 2019, Macau, Macao; pp. 161–164. https://doi.org/10.1109/A-SSCC47793.2019.9056980.
299. Urain, A.; del Rio, D.; Gurutzeaza, I.; Solar, H.; Beriain, A.; Berenguer, R. Design and Layout Considerations of a D-Band SiGe LNA for Radiometric Applications. In Proceeding of the 2021 XXXVI Conference on Design of Circuits and Integrated Systems (DCIS), 24-26 November 2021, Vila do Conde, Portugal; pp. 1–5. https://doi.org/10.1109/DCIS53048.2021.9666165.
300. Aksoyak, Í.K.; Möck, M.; Ulusoy, A.Ç. A Differential D-Band Low-Noise Amplifier in 0.13 μm SiGe. *IEEE Microwave and Wireless Components Letters*. **2022**, *32*, 979–982. https://doi.org/10.1109/LMWC.2022.3164255.
301. Dacquay, E.; Tomkins, A.; Yau, K. H. K.; Laskin, E.; Chevalier, P.; Chantre, A.; Sautreuil, B.; Voinigescu, S. P.; *D* -Band Total Power Radiometer Performance Optimization in an SiGe HBT Technology. *IEEE Microw. Wirel. Components Lett.* **2012**, *60*, 813–826. https://doi.org/10.1109/TMTT.2012.2184132.
302. Stärke, P.; Fritsche, D.; Carta, C.; Ellinger, F. A 24.7 dB low noise amplifier with variable gain and tunable matching in 130 nm SiGe at 200 GHz. In Proceeding of the 2017 12th European Microwave Integrated Circuits Conference (EuMIC), 8-10 October 2017, Nuremberg, Germany; pp. 5–8. https://doi.org/10.23919/EuMIC.2017.8230646.
303. Danneville, F.; Deng, M.; Bouvot, S.; Azevedo Goncalves, J.; Lépilliet, S.; Ducournau, G.; Gaquière, C.; Dambrine, G.; Bossuet, A.; Quémerais, T.; et al. Noise parameters of SiGe HBTs in mmW range: Towards a full in situ measurement extraction. In Proceeding of the 2017 International Conference on Noise and Fluctuations (ICNF), 20-23 June 2017, Vilnius, Lithuania; pp. 1–4. https://doi.org/10.1109/ICNF.2017.7985944.
304. Azevedo Gonçalves, J. C.; Ghanem, H.; Bouvot, S.; Gloria, D.; Lépilliet, S.; Ducournau, G.; Gaquière, C.; Danneville, F. Millimeter-Wave Noise Source Development on SiGe BiCMOS 55-nm Technology for Applications up to 260 GHz. *IEEE Microw. Wirel. Components Lett.* **2019**, *67*, 3732–3742. https://doi.org/10.1109/TMTT.2019.2926289.
305. Kanar, T.; Rebeiz, G.M. A low-power SiGe D-band total power radiometer with NEPmin of 1.4 fW/Hz½ and NETD of 0.25K. In Proceeding of the 2016 IEEE MTT-S International Microwave Symposium (IMS), 22-27 May 2016, San Francisco, CA, USA; pp. 1–4. https://doi.org/10.1109/MWSYM.2016.7540359.
306. Parveg, D.; Varonen, M.; Kärkkäinen, M.; Karaca, D.; Vahdati, A.; Halonen, K.A.I. Wideband millimeter-wave active and passive mixers in 28 nm bulk CMOS technology. In Proceeding of the 2015 10th European Microwave Integrated Circuits Conference (EuMIC), 7-8 September 2015, Paris, France; pp. 116–119. https://doi.org/10.1109/EuMIC.2015.7345082.
307. Aroca, R.A.; Tomkins, A.; Doi, Y.; Yamamoto, T.; Voinigescu, S.P. Circuit performance characterization of digital 45-nm CMOS technology for applications around 110 GHz. In Proceeding of the 2008 IEEE Symposium on VLSI Circuits, 18-20 June 2008, Honolulu, HI, USA; pp. 162–163. https://doi.org/10.1109/VLSIC.2008.4585991.
308. Bouvot, S.; Quémerais, T.; Azevedo Goncalves, J. C.; Lépilliet, S.; Ducournau, G.; Danneville, F.; Gloria, D. A D-band passive receiver with 10 dB noise figure for in-situ noise characterization in BiCMOS 55 nm. In Proceeding of the 2017 IEEE 17th Topical Meeting on Silicon Monolithic Integrated Circuits in RF Systems (SiRF), 15-18 January 2017, Phoenix, AZ, USA; pp. 107–110. https://doi.org/10.1109/SIRF.2017.7874385.
309. Aouimeur, W.; Gaquière, C.; Lauga-Larroze, E.; Arnould, J.-D.; Moron-Guerra, J.; Quemerais, T.; Gloria, D.; Serhan, A. A Fully In-Situ Reflectometer in G band in 55 nm SiGe BiCMOS. In Proceeding of the 2018 International Workshop on Integrated Nonlinear Microwave and Millimetre-wave Circuits (INMMIC), 5-6 July 2018, Brive La Gaillarde, France; pp. 1–3. https://doi.org/10.1109/INMMIC.2018.8430015.
310. Liu, Y.; Wen, J.; Wang, L. A D-Band Down-Conversion Mixer Based on 65 nm CMOS Technology. In Proceeding of the 2018 International Applied Computational Electromagnetics Society Symposium-China (ACES), 29 July - 1 August 2018, Beijing, China; pp. 1–2. https://doi.org/10.23919/ACESS.2018.8669277.
311. Lee, C.J.; Park, C.S. A D-Band Gain-Boosted Current Bleeding Down-Conversion Mixer in 65 nm CMOS for Chip-to-Chip Communication. *IEEE Microw. Wirel. Components Lett.* **2016**, *26*, 143–145. https://doi.org/10.1109/LMWC.2016.2517132.

312. Yoon, D.; Kim, N.; Song, K.; Kim, J.; Oh, S.J.; Rieh, J.-S. D-Band Heterodyne Integrated Imager in a 65-nm CMOS Technology. *IEEE Microw. Wirel. Components Lett.* **2015**, *25*, 196–198. https://doi.org/10.1109/LMWC.2015.2390496.
313. Hung, S.; Cheng, K.; Wang, Y. An Ultra-Broadband Subharmonic Mixer With Distributed Amplifier Using 90-nm CMOS Technology. *IEEE Microw. Wirel. Components Lett.* **2013**, *61*, 3650–3657. https://doi.org/10.1109/TMTT.2013.2277993.
314. Wang, Y. A novel D-band sub-harmonic I/Q modulator based on diodes. In Proceeding of the 2020 International Conference on Information Science, Parallel and Distributed Systems (ISPDS), 14-16 August 2020, Xi'an, China; pp. 65–68. https://doi.org/10.1109/ISPDS51347.2020.00021.
315. Ning, X.; Yao, H.; Wu, D.; Su, Y.; Jin, Z. An 89 GHz single-balanced mixer design in 1 um InP DHBT technology. 2015 Asia-Pacific Microwave Conference (APMC), 2015; pp. 1–3. https://doi.org/10.1109/APMC.2015.7413549.
316. Hassona, A.; Vassilev, V.; Zirath, H. G-band Frequency Converters in 130-nm InP DHBT Technology. In Proceeding of the 2020 50th European Microwave Conference (EuMC), 12-14 January 2021, Utrecht, Netherlands; pp. 1027–1030. https://doi.org/10.23919/EuMC48046.2021.9338049.
317. Yan, Y.; Bao, M.; Gunnarsson, S.E.; Vassilev, V.; Zirath, H. A 110–170-GHz Multi-Mode Transconductance Mixer in 250-nm InP DHBT Technology. *IEEE Microw. Wirel. Components Lett.* **2015**, *63*, 2897–2904. https://doi.org/10.1109/TMTT.2015.2459676.
318. Carpenter, S.; Abbasi, M.; Zirath, H. Fully Integrated D-Band Direct Carrier Quadrature (I/Q) Modulator and Demodulator Circuits in InP DHBT Technology. *IEEE Microw. Wirel. Components Lett.* **2015**, *63*, 1666–1675. https://doi.org/10.1109/TMTT.2015.2409831.
319. McCue, J.J.; Casto, M.; Li, J.C.; Watson, P.; Khalil, W. An Active Double-Balanced Down-Conversion Mixer in InP/Si BICMOS Operating from 70–110 GHz. In Proceeding of the 2014 IEEE Compound Semiconductor Integrated Circuit Symposium (CSICS), 19-22 October 2014, La Jolla, CA, USA; pp. 1–4. https://doi.org/10.1109/CSICS.2014.6978540.
320. Karandikar, Y.; Zirath, H.; Yan, Y.; Vassilev, V. Compact Integration of Sub-Harmonic Resistive Mixer with Differential Double Slot Antenna in G-Band Using 50nm InP-HEMT MMIC Process. In Proceeding of the 2012 IEEE Compound Semiconductor Integrated Circuit Symposium (CSICS), 14-17 October 2012, La Jolla, CA, USA; pp. 1–5. https://doi.org/10.1109/CSICS.2012.6340081.
321. Maiwald, T.;Potschka, J.; Kolb, K.; Dietz, M.; Hagelauer, A.; Visweswaran, A.; Weigel, R. A Broadband Zero-IF Down-Conversion Mixer in 130 nm SiGe BiCMOS for Beyond 5G Communication Systems in D-Band. *IEEE Trans. Circuits Syst. II Express Briefs* **2021**, *68*, 2277–2281. https://doi.org/10.1109/TCSII.2021.3053344.
322. Ahmed, F.; Furqan, M.; Heinemann, B.; Stelzer, A. A SiGe-based broadband 140–170-GHz downconverter for high resolution FMCW radar applications. In Proceeding of the 2016 IEEE MTT-S International Conference on Microwaves for Intelligent Mobility (ICMIM), 19-20 May 2016, San Diego, CA, USA; pp. 1–4. https://doi.org/10.1109/ICMIM.2016.7533917.
323. Seyedhosseinzadeh, N.; Nabavi, A.; Carpenter, S.; He, Z.S.; Bao, M.; Zirath, H. A 100–140 GHz SiGe-BiCMOS sub-harmonic down-converter mixer. In Proceeding of the 2017 12th European Microwave Integrated Circuits Conference (EuMIC), 8-10 October 2017, Nuremberg, Germany; pp. 17–20. https://doi.org/10.23919/EuMIC.2017.8230649.
324. Hu, S.; Xiong, Y.; Wang, L.; Shi, J.; Lim, T. A 77–135GHz down-conversion IQ mixer for 10Gbps multiband applications. In Proceedings of the 2011 International Symposium on Integrated Circuits, 12-14 December 2011, Singapore; pp. 29–34. https://doi.org/10.1109/ISICir.2011.6131872.
325. Hu, S.; Xiong, Y.-Z.; Wang, L.; Zhang, B. A 135GHz single-ended mixer in 0.13μm SiGe HBT for high-speed demodulation. In Proceeding of the 2012 IEEE International Symposium on Radio-Frequency Integration Technology (RFIT), 21-23 November 2012, Singapore; pp. 53–55. https://doi.org/10.1109/RFIT.2012.6401611.
326. Zhang, Y.; Liang, W.; Sakalas, P.; Mukherjee, A.; Jin, X; Krause, J.; Schröter, M. 12-mW 97-GHz Low-Power Downconversion Mixer With 0.7-V Supply Voltage. *IEEE Microw. Wirel. Components Lett.* **2019**, *29*, 279–281. https://doi.org/10.1109/LMWC.2019.2901410.
327. Bilato, A.; Issakov, V.; Mazzanti, A.; Bevilacqua, A. A Multichannel D-Band Radar Receiver With Optimized LO Distribution. *IEEE Solid-State Circuits Letters*, **2021**, *4*, 141–144. https://doi.org/10.1109/LSSC.2021.3099069.
328. Kuo, J.-J.; Chun-Hsien, L.; Lin, K.; Schmalz, K.; Scheytt, J. C.; Huei, W. Design and Analysis of Down-Conversion Gate/Base-Pumped Harmonic Mixers Using Novel Reduced-Size 180° Hybrid With Different Input Frequencies. *IEEE Trans. Microw. Theory Tech.* **2012**, *60*, 2473–2485. https://doi.org/10.1109/TMTT.2012.2202039.
329. Lal, D.; Abbasi, M.; Ricketts, D.S. A broadband, compact 140–170GHz double side-band receiver in 90nm SiGe technology. In Proceeding of the 2016 46th European Microwave Conference (EuMC), 4-6 October 2016, London, UK; pp. 687–690. https://doi.org/10.1109/EuMC.2016.7824436.